Neurochemical Research
https://doi.org/10.1007/s11064-020-03148-2

ORIGINAL PAPER

Cinnamoyl-*N*-Acylhydrazone-Donepezil Hybrids: Synthesis and Evaluation of Novel Multifunctional Ligands Against Neurodegenerative Diseases

Cindy Juliet Cristancho Ortiz[1] · Caio Miranda Damasio[1] · Letizia Pruccoli[2] · Nathália Fonseca Nadur[3] · Luciana Luiza de Azevedo[3] · Isabella Alvim Guedes[4] · Laurent Emmanuel Dardenne[4] · Arthur Eugen Kümmerle[3] · Andrea Tarozzi[2] · Claudio Viegas Jr.[1]

Received: 23 July 2020 / Revised: 25 September 2020 / Accepted: 7 October 2020

Abstract

A new series of ten multifunctional Cinnamoyl-*N*-acylhydrazone-donepezil hybrids was synthesized and evaluated as multifunctional ligands against neurodegenerative diseases. The molecular hybridization approach was based on the combination of 1-benzyl-4-piperidine fragment from the anti-Alzheimer AChE inhibitor donepezil (**1**) and the cinnamoyl subunit from curcumin (**2**), a natural product with remarkable antioxidant, neuroprotective and anti-inflammatory properties, using a *N*-acylhydrazone fragment as a spacer subunit. Compounds **4a** and **4d** showed moderate inhibitory activity towards AChE with IC_{50} values of 13.04 and 9.1 µM, respectively. In addition, compound **4a** and **4d** showed a similar predicted binding mode to that observed for donepezil in the molecular docking studies. On the other hand, compounds **4a** and **4c** exhibited significant radical scavenging activity, showing the best effects on the DPPH test and also exhibited a significant protective neuronal cell viability exposed to t-BuOOH and against 6-OHDA insult to prevent the oxidative stress in Parkinson's disease. Similarly, compound **4c** was capable to prevent the ROS formation, with indirect antioxidant activity increasing intracellular GSH levels and the ability to counteract the neurotoxicity induced by both OAβ1-42 and 3-NP. In addition, ADMET in silico prediction indicated that both compounds **4a** and **4c** did not show relevant toxic effects. Due to their above-mentioned biological properties, compounds **4a** and **4c** could be explored as lead compounds in search of more effective and low toxic small molecules with multiple neuroprotective effects for neurodegenerative diseases.

Graphic Abstract

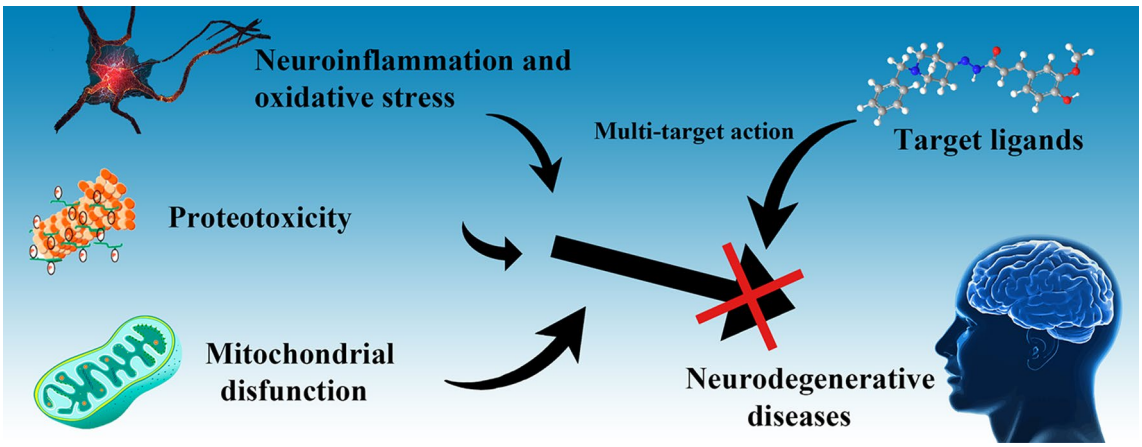

Electronic supplementary material The online version of this article (https://doi.org/10.1007/s11064-020-03148-2) contains supplementary material, which is available to authorized users.

Extended author information available on the last page of the article

Published online: 20 October 2020

Keywords Cinnamoyl-*N*-acylhydrazone-donepezil hybrids MTDLs · Multifunctional ligands · Neurodegenerative diseases · Molecular hybridization

Introduction

Neurodegenerative diseases (NDs), including Alzheimer's disease (AD), Parkinson's disease (PD), Huntington's disease (HD), and amyotrophic lateral sclerosis, are a heterogeneous group of neurological disorders caused by the progressive death of neurons in different regions of the nervous system, leading to locomotion and behavior impairments, cognitive decline and dementia, that affect millions of people worldwide. In particular, AD is characterized by the formation of senile plaques and neurofibrillary tangles in the cerebral cortex as well as neuron and synapse loss. Similarly, PD is associated with dopaminergic neuronal death and formation of Lewy bodies due to the deposition of the protein α-synuclein that leads to dysfunction in the regulation of major brain structures involved in the movement control. Although the available treatments may help to alleviate progression and some symptoms associated with NDs, such as donepezil, rivastigmine, galanthamine and memantine for AD [1, 2] or

Levodopa to PD [3], there is currently no way to effective blockade disease progression and cure [4]. Ageing is the major risk factor for neurodegeneration [5]. Nonetheless, there are some intrinsic factors such as genetic, epigenetic and brain damage associated with neuroinflammation, oxidative stress, as well as lifestyle factors, including diets rich in sugar and fat foods, alcohol and tobacco dependence [6]. Neurodegeneration is also correlated with an imbalanced production of free radicals from enzyme activity, mitochondrial impairment, and decreased activity of the antioxidant system. The excessive production of reactive oxygen species (ROS) causes oxidative stress, increasing the risk of developing NDs. Such radical species may react with different functional groups from endogen molecules, including bases in nucleic acids, amino acid side chains in proteins and double bonds in unsaturated fatty acids, which can damage DNA, RNA, proteins and lipids [7]. Antioxidant compounds such as curcumin can decrease the oxidative damage directly, via reacting with free radicals, or indirectly, exerting their antioxidant effects by inducing cytoprotective phase 2 genes and improving intracellular antioxidant enzymes [8].

Currently, the available treatments for NDs, especially for AD and PD, are only restricted to symptoms alleviation and curb disease progression and severity, with drugs acting specifically over single molecular targets. In the case of AD, galanthamine, donepezil and rivastigmine are AChE inhibitors and memantine acts as glutamate-related NMDA receptor antagonist, whereas PD has been treated by tentative restoring of the dopaminergic system. Considering the lack in efficacy and the multifactorial complexity related to the pathophysiology of NDs, it is urgent the adoption of other therapeutic approaches such as multifunctional or multi-target directed ligands (MTDLs) strategy [9]. Based on polypharmacology concept, the MTDLs approach advocates that better therapeutical results could be achieved by a single molecule that could concomitantly modulate more than one molecular target associated with NDs pathophysiology. Despite better pharmacodynamics, the use of multifunctional drugs could avoid adverse effects, deleterious drug–drug interactions, and metabolic stress. The rationale behind the structural design of these new multifunctional chemical entities uses the molecular hybridization as its main tool, combining different structural patterns or structural fragments from two or more known bioactive molecules into a new single molecular skeleton capable of reproducing the original properties of the prototype molecules [10]. The MTDLs approach represents an interesting strategy for the development of drug candidates that have antioxidant and neuroprotective effects, enzyme inhibitory properties and can effectively penetrate the CNS barrier and restore cognition, memory functions and brain homeostasis [11].

In a previous work [12], we reported the synthesis and biological evaluation of a series of feruloyl-donepezil hybrid compounds designed as multitarget drug candidates for AD treatment. Some of those compounds showed significant neuroprotective properties in human neuronal cells against oxidative damage, anti-inflammatory properties, and potent AChE inhibitory activity. On the other hand, the use of *N*-acylhydrazones (NAHs) and their derivatives has been reported in the literature as important privileged structures, with important biological potential in bioactive ligands of different pharmacological profiles [13]. NAHs are characterized by being able to contribute to molecular recognition for a wide number of biological targets, whose structural modification of their substituents can result in compounds with great biological potential. In addition, NAHs could also contribute for improving pharmacokinetic properties due to its higher polarity, with donor and acceptor hydrogen bond sites, allowing additional molecular interactions [14]. Considering the promising results evidenced by our group in earlier studies, exploring the pharmacophoric contribution of the NAH substructure, the anticholinesterase properties of the *N*-benzylpiperidine fragment from donepezil (**1**), we designed another series of donepezil-based *N*-acylhydrazone hybrids (**4a-j**, Fig. 1) based on the combination of 1-benzyl-4-piperidine system and the cinnamoyl subunit from curcumin (**2**) and ferulic acid

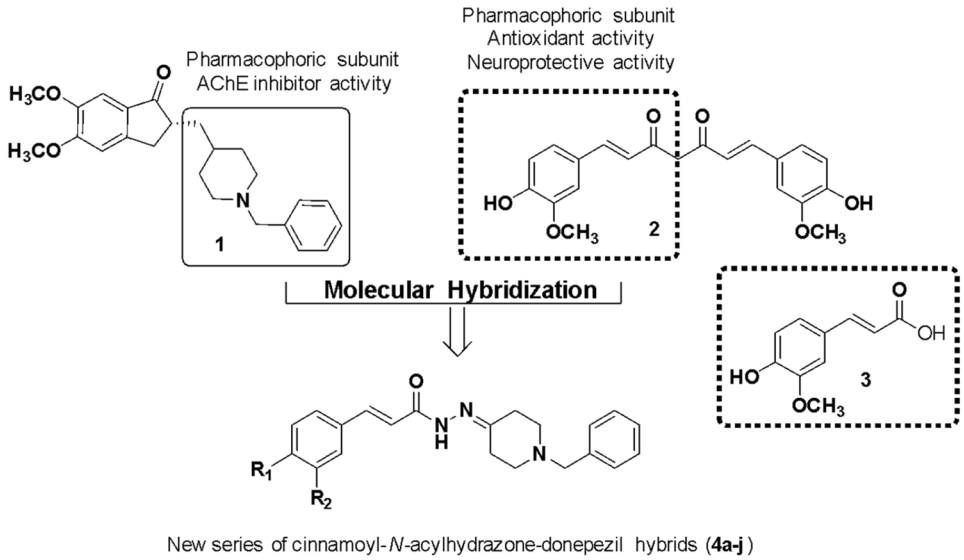

Fig. 1 Design of a new series of cinnamic-*N*-acylhydrazone-donepezil hybrids (**4a-j**)

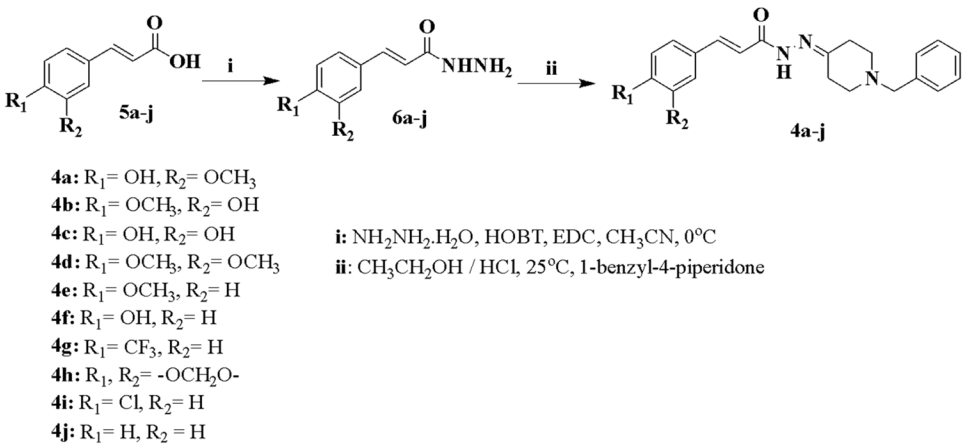

Fig. 2 Synthetic route for the preparation of the cinnamoyl-*N*-acylhydrazone-donepezil hybrids **4a-j**

(**3**), two known natural products with antioxidant, neuroprotective and anti-inflammatory properties, using a *N*-acylhydrazone subunit as spacer. By this proposal, the *N*-benzyl-4-piperidine subunit was elected as a suitable mimic of the AChE inhibitor pharmacophore *N*-benzylpiperidine fragment from **1**, conserving the Nitrogen atom as a protonable site and inserting a relative conformational restriction imposed by the exocyclic double bond at the hydrazone functionality. Moreover, different substituents at the cinnamoyl fragment could be interesting in a SAR study and their role in the desired antioxidant and neuroprotective properties, leading to the identification of new multifunctional ligands with an innovative scaffold, suitable for pharmaceutical development for AD treatment.

The synthesis of the target-compounds **4a-j** was based on the preparation of the key-hydrazide intermediates **6a-j** from cinnamic acid derivatives **5a-j** (Fig. 2). The starting carboxylic acids were reacted with hydrazine hydrate

Table 1 Experimental data for compounds **4a-j**

Compound	R_1	R_2	Yield (%)	MP (°C)†	Purity (%)
263 (4a)	OH	OCH_3	46	203	100
264 (4b)	OCH_3	OH	37	192	100
265 (4c)	OH	OH	19	140	98,81
266 (4d)	OCH_3	OCH_3	55	185	100
267 (4e)	OCH_3	H	29	>300	99,33
268 (4f)	OH	H	39	226	100
269 (4 g)	CF_3	H	57	188	99,99
270 (4 h)	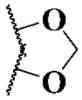		56	90	100
271 (4i)	Cl	H	73	209	100
272 (4j)	H	H	11	183	100

†: Melting point

in the presence of HOBT and EDC to provide the desired compounds **4a-j**. Then, these hydrazide intermediates were coupled to 1-benzyl-4-piperidone, leading to the desired cinnamoyl-donepezil hybrids **4a-j** in global yields of 11–73% (Table 1). All compounds were characterized by IR, NMR and HRMS techniques. The purity of compounds was determined by HPLC.

In Vitro Inhibition of AChE and BuChE

Cholinesterase (ChE) inhibitors are effective in improving behavior, memory, well-being and reducing cognitive decline in patients with dementia. Thus, the modified Ellman's method [15] was used to determine the inhibitory profile of the cinnamoyl-*N*-acylhydrazone-donepezil hybrids against AChE and BuChE enzymes. Preliminary results showed that compounds **4a-j** were capable to inhibit AChE in a range of 47–76% at 30 µM. Additionally, at the same concentration, some compounds could also inhibit BuChE in a range of 62–82% (Table 2).

Most of the target-compounds showed moderate inhibitory activity towards AChE or BuChE, indicating that the introduction of *N*-benzyl-piperidine fragment was determinant for inhibition of ChEs, which results are shown in Table 2. Compounds with ChE inhibition higher than 45% have their IC_{50} values determined, highlighting compound PQM-266 (**4d**) as the most potent and selective AChE inhibitor with $IC_{50} = 9.1$ µM, followed by compounds PQM-263 (**4a**), PQM-264 (**4b**) and PQM-270 (**4 h**), with IC_{50} values of 13.04, 17.04 and 19.44 µM, respectively, with no significant activity over BuChE. Conversely, compound PQM-272 (**4j**) with $IC_{50} = 11.94$ µM showed to be the most potent BuChE inhibitor, followed by PQM-271 (**4i**) and PQM-268 (**4f**), with IC_{50} values of 14.44 and 14.42 µM, respectively. It is interesting to note that only compound PQM-271 (**4i**) showed significant inhibition of both enzymes, whereas the most potent and selective AChE inhibitors did not showed activity against BuChE and vice versa. This selective profile in ChE inhibition could be useful in the development of drug candidates for AD treatment, since in the most advanced stages of AD, ACh is mainly hydrolyzed by BuChE, that is indicative of an increase in BuChE activity, leading to a decrease in ACh level in the late stage of AD. Hence, the development of selective BuChE inhibitors, such as PQM-272 (**4j**) may represent an interesting therapeutic strategy [16]. In fact, almost all drugs approved for AD management worldwide are selective AChE inhibitors, with rivastigmine being the only one dual AChE/BuChE inhibitor currently FDA-approved for the treatment of mild, moderate and severe AD and mild to moderate PD, demonstrating improvement in the cognitive condition of patients [17]. In contrast, dual AChE/BuChE inhibitors such as PQM-271 (**4i**) may also be considered as a therapeutic advantage for cortical dementias, such as AD and PD, benefiting cognition and treating behavioral symptoms. A SAR analysis evidenced that most potent AChE inhibitors were compounds with 3,4-di-oxygenated substituents at the cinnamoyl subunit, whereas the best BuChE inhibitors have no *O*-substituent on that fragment. Moreover, the replacement of the 3,4-dihydroxyl groups in PQM-265 (**4c**) for a 3,4-*di*-methoxyl groups in PQM-266 (**4d**) significantly increased the inhibitory potency and selectivity against AChE. However, the influence of the substituents at the cinnamoyl fragment on BuChE activity was the opposite, suggesting that the absence of substituents increases both inhibition potency

Table 2 Experimental data of in vitro inhibition of AChE and BuChE, DPPH radical scavenging activity and cell viability for compounds **4a-j**

Compounds	*Ee*AChE		*eq*BuChE		% Inhibition of DPPH radical (at 80 µM)	% cell viability (at 80 µM)[†]
	% inhibition (at 30 µM)	$IC_{50} \pm SD$ (30 µM)	% Inhibition (at 30 µM)	$IC_{50} \pm SD$ (30 µM)		
PQM-263 (**4a**)	47.1	13.04 ± 0.41	29.3	NA	53.37	99.88
PQM-264 (**4b**)	55.9	17.40 ± 0.32	23.9	NA	6.84	92.43
PQM-265 (**4c**)	43.0	NA	62.0	21.99 ± 1.58	45.05	63.85
PQM-266 (**4d**)	75.6	9.10 ± 0.68	3.4	NA	− 1.41	80.70
PQM-267 (**4e**)	10.5	NA	1.8	NA	2.59	114.31
PQM-268 (**4f**)	32.5	NA	69.9	14.42 ± 0.48	2.33	73.59
PQM-269 (**4 g**)	49.4	30.07 ± 0.63	43.0	NA	13.70	127.28
PQM-270 (**4 h**)	47.3	19.44 ± 1.28	27.5	NA	− 3.05	92.48
PQM-271 (**4i**)	58.4	31.52 ± 2.28	64.5	13.44 ± 0.83	8.78	81.84
PQM-272 (**4j**)	23.2	NA	82.5	11.94 ± 0.65	− 2.56	77.33

IC_{50}: compound concentration required to produce the 50% of inhibition, data were shown in mean ± SD of triplicate of independent experiments

NA No active, inhibition 45% at 30 µM

[a]Cell viability percentage at the maximum concentration by MTT assay

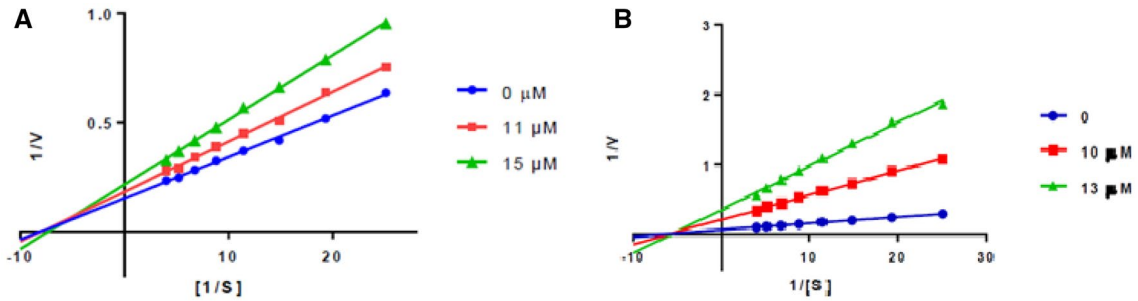

Fig. 3 Lineweaver-Burk plots for **a** AChE inhibition by PQM-263 (**4a**) and **b** BuChE inhibition by compound PQM-272 (**4j**)

Table 3 Kinetic parameters of compound PQM-263 (**4a**) against AChE

Concentration (µM)	$V_{max} \pm SD^a$ (µM/min)	$K_m \pm SD^b$ (µM)	K_i (µM) $\pm SD^c$	$K_{i'}$ (µM) $\pm SD^d$
0	7.15 ± 0.495	133.90 ± 1.41	19.04 ± 0.823	40.31 ± 1.628
11	5.88 ± 0.207	148.35 ± 2.47		
15	6.39 ± 0.276	228.00 ± 13.0		

[a]Maximum velocity of the enzyme

[b]Michaelis constant

[c]Competitive constant

[d]Non-competitive constant; data were shown in mean ± SD of triplicate of independent experiments

Table 4 Kinetic parameters of compound PQM-272 (**4j**) against BuChE

Concentration (µM)	$V_{max} \pm SD^a$ (µM/min)	$K_m \pm SD^b$ (µM)	K_i (µM) $\pm SD^c$	$K_{i'}$ (µM) $\pm SD^d$
0	16.09 ± 0.292	152.93 ± 0.28	1.62 ± 0.020	3.35 ± 0.039
10	5.17 ± 0.288	191.75 ± 3.18		
13	3.14 ± 0.136	247.75 ± 1.34		

[a]Maximum velocity of the enzyme

[b]Michaelis constant

[c]Competitive constant

[d]Non-competitive constant; data were shown in mean ± SD of triplicate of independent experiments

and selectivity for BuChE as evidenced by compound PQM-272 (**4j**), which has no substituents on the aromatic ring.

In order to gain insight into the mechanism of AChE and BuChE inhibition, the compounds PQM-263 (**4a**) and PQM-272 (**4j**) were selected for kinetic studies for the AChE and BuChE, respectively. The Lineweaver–Burk plots (Fig. 3) evidenced a mixed-type mechanism of inhibition by both compounds tested, suggesting that the inhibitors are capable of binding both to the catalytic (competitive inhibition) and to the allosteric (non-competitive inhibition) sites of both enzymes. The inhibition constants were calculated, and kinetic parameters are shown in Tables 3 and 4.

Table 5 Docking results for the compounds 4a-4j against AChE (PDB code 4EY7) and BuChE (PDB code 6I0C)

Compound	AChE score (kcal/mol)	BuChE score (kcal/mol)
PQM-263 (**4a**)	− 9.7	− 7.3
PQM− 264 (**4b**)	− 8.9	− 7.0
PQM− 265 (**4c**)	− 8.8	− 7.3
PQM− 266 (**4d**)	− 10.26	− 7.0
PQM− 267 (**4e**)	− 8.8	− 7.1
PQM− 268 (**4f**)	− 11.0	− 7.2
PQM-269 (**4 g**)	− 9.6	− 6.6
PQM− 270 (**4 h**)	− 9.2	− 6.9
PQM− 271 (**4i**)	− 9.1	− 6.8
PQM− 272 (**4j**)	− 8.5	− 8.1
Donepezil	− 12.2	− 7.6

Molecular Docking Study with AChE

The docking results for the AChE and BuChE are shown in Table 5. The compounds PQM-268 (**4f**), PQM-266 (**4d**) and PQM-263 (**4a**) were predicted as the most potent inhibitors against AChE, whereas the compound **4j** was the only compound predicted to inhibit the BuChE with binding affinity better than – 8 kcal/mol. From these results, only the compound PQM-268 (**4f**) did not exhibit in vitro activity against the respective enzyme.

The predicted binding modes for PQM-263 (**4a**) and PQM-266 (**4d**) are similar to that observed for donepezil (Fig. 4a), being characterized by: (i) π-stacking interaction between the phenyl ring with the Trp86 indole ring, (ii) cation-π interaction of the piperidine group with the Tyr337 side chain, (iii) hydrogen bond between the carbonyl oxygen of the NAH group with the Tyr121 side chain, and (iii) hydrophobic interactions between the 1,2-dimethoxybenzene and the PAS region, and (iv) hydrophobic interactions between the methoxy at the *meta*-position with the Trp286 and Tyr72 side chains from the PAS (Fig. 4b, PQM-266 not shown). According to the docking results, the dimethoxybenzene and hydroxymethoxybenzene groups from these compounds are not able to perform the optimal stacking interactions with Trp279 observed for donepezil, probably due to the slightly longer linker moiety of the NAH derivative. Furthermore, the methoxy group of these compounds are more exposed to the solvent than in the donepezil experimental binding mode. However, since the PAS region is highly flexible, it is possible that the AChE can adjust this region to accommodate the compounds PQM-263 (**4a**) and PQM-266 (**4d**) through an induced-fit mechanism, providing optimal hydrophobic and stacking interaction with PAS.

For the BuChE, the compound with the best predicted affinity was PQM-272 (**4j**), which was also experimentally active against the enzyme. The superposition of the predicted binding mode PQM-272 with the cognate ligand of the complex 6I0C exhibited some similar interactions that may justify its potency, being characterized by: (i) π-stacking

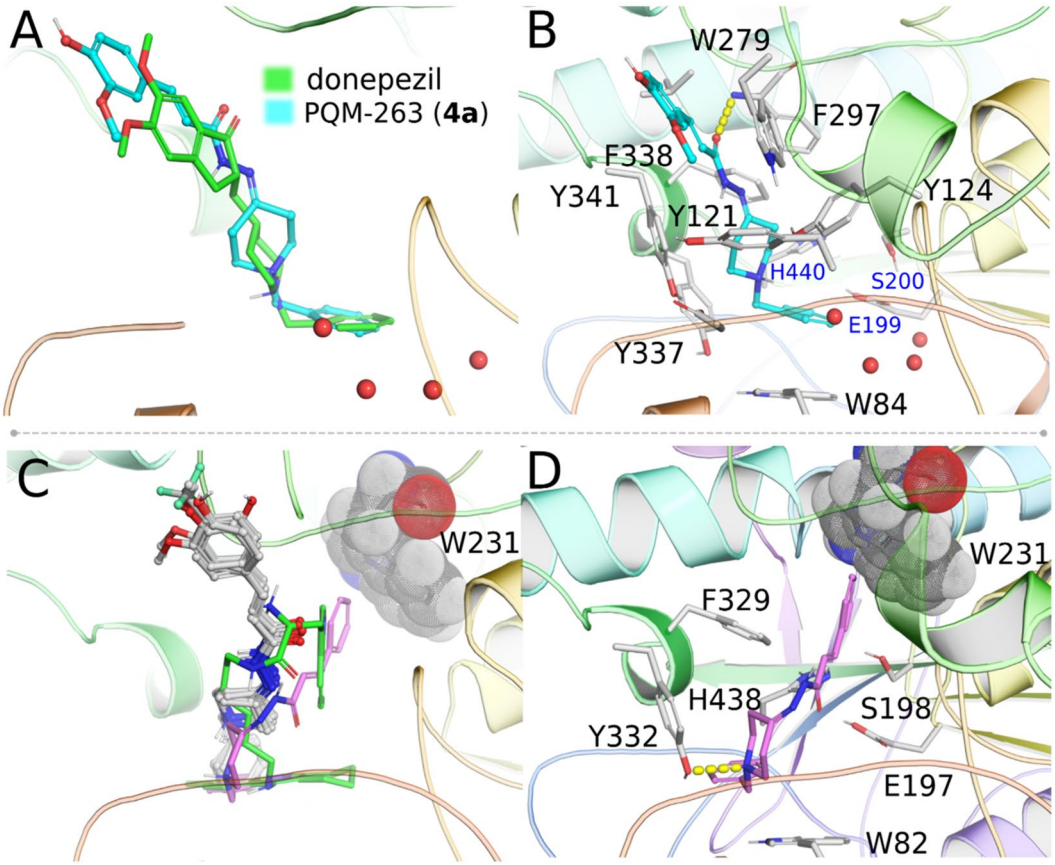

Fig. 4 Top-energy predicted binding mode of **a** PQM-263 (**4a**) superimposed with donepezil, **b** PQM-263 (**4a**) interacting with the AChE binding site (PDB code 4EY7), **c** cinnamoyl derivatives superimposed with the co-crystallized ligand of the BuChE structure 6I0C, and **d** PQM-272 (**4j**) interacting with the BuChE binding site (PDB code 6I0C). Hydrogen bonds are represented as yellow dashes and BuChE Trp231 is highlighted as dots. The co-crystallized ligands are colored green, PQM-263 (**4a**) is colored cyan and PQM-272 (**4j**) is colored pink

interaction between the phenyl group of the *N*-benzyl-piperidine moiety with the Trp82 indole ring, (ii) hydrogen bond between the positively charged nitrogen from the piperidine ring with the Try332 side chain, and (iii) T-stacking interaction between the phenyl ring from the cinnamoyl fragment and the Trp231 side chain (Fig. 4c, d). It is important to highlight that the Trp231 is only accessible in the BuChE due to the substitution of Phe295 in AChE to Val288, providing enough room to aromatic fragments interacting with this hydrophobic pocket [16, 18–22]. This hypothesis is reinforced by the SAR of our compounds, which demonstrated that substitutions at the phenyl ring from the cinnamoyl fragment led to reduced potency and selectivity.

In fact, only the compound PQM-272 (**4j**) from the cinnamoyl derivatives was able to interact with Trp231 (Fig. 4c). These findings provide useful insights for further molecular optimizations of the cinnamoyl derivatives to obtain more potent and selective compounds.

In Vitro Antioxidant Activity Evaluation

Oxidative stress is a common feature in NDs, which demands an abnormal increase in free radical generation in the brain, along with cytotoxicity, leading to mitochondrial dysfunction, neuronal cell death and altered synaptic function [23]. There is a number of evidences in the literature that curcumin and its derivatives, such as ferulic acid, protect neurons from injury by preventing free radical-mediated neuroinflammation implicated in the pathology of NDs and contribute to memory improvement [24, 25].

Considering the oxidative damage associated with NDs, compounds **4a-j** were evaluated for their in vitro antioxidant activity by DPPH assay, in different concentrations (1.56–200 µM) and in triplicate. DPPH (2,2-diphenyl-1-picrylhydrazyl) radicals can be used in preliminary screening of scavenging reactive oxygen species (ROS). The radical scavenging capacity was represented as a percentage of the DPPH radical scavenging activity at 80 µM of concentration and the results are shown in Table 2. The ferulic acid-based hybrid PQM-263 (**4a**) was more effective than the *iso*-ferulic derivative PQM-264 (**4b**) and the strongest antioxidant in the series, inhibiting 53.37% of DPPH radicals at 80 µM, followed by PQM-265 (**4c**) that inhibited 45.05% of DPPH radicals at the same concentration. These results evidenced that all compounds without a phenolic hydroxyl group lack in antioxidant activity, which indicates that radical scavenging activity depends on the number and position of hydroxy and methoxy substituents attached to the aromatic ring and that the *para*-hydroxy substituent is determinant for antioxidant efficacy [12, 26]. Therefore, the ferulic acid pattern is the most adequate pattern for cinnamic the strongest antioxidant ability, probably due to the formation of a phenolic radical that can be stabilized through conjugation extension. When the radical is located at the meta-position, the oxygen atom is unable to share the charge, affecting antioxidant capacity, which could be evidenced in the mono-hydroxycinnamic derivative PQM-268 (**4f**) that exhibited very weak antiradical activity, but methoxy group improved the activity as evidenced for compound PQM-263 (**4a**) [12, 26].

Evaluation of Cytotoxicity and Antioxidant Properties by Cell-Based Assay

The new compounds have been designed to have a multifunctional profile using fragments of donepezil and curcumin. By contrast to curcumin, donepezil is commercial drug with a known pharmacological mechanism. Therefore, we used donepezil in various experiments with cells. The donepezil did not show the ability to counteract the oxidative stress confirming its selective action only on acetylcholinesterase activity. We added this information in (Figs. 5 and 6). At this point, with the current level of drug discovery, we evaluated only some aspects of pharmacokinetic and toxicity by ADME studies. The previous information was reported in Table 6.

Subsequently, we evaluated the neurotoxicity of all target-compounds in human neuronal (SH-SY5Y) cells by MTT assay. After testing compounds **4a-j** at eight different concentrations from 2.5 to 80 µM, in triplicate, no significant cytotoxicity was observed at the maximum concentration of 80 µM (Table 2). In parallel, we selected the best dual ChE inhibitors and antioxidants PQM-263 (**4a**), PQM-264 (**4b**), PQM-265 (**4c**) and PQM-266 (**4d**) for evaluating their ability to inhibit the intracellular ROS formation induced by *t*-BOOH in SH-SY5Y cells. Initially, the evaluation was performed by a co-treatment approach, that is, the target-substances and *t*-BOOH were administered at the same time. In this regard, this approach allows to evaluate the direct antioxidant activity of the compounds in SH-SY5Y cells. In Fig. 5a, the results are shown in percentage inhibition of ROS formation in relation to exposed cells only with *t*-BOOH, and except for **4d**, all other target-compounds showed significant antioxidant effects against oxidative damage induced by *t*-BOOH at 2.5, 5 and 10 µM. These results corroborated the significant radical scavenging activity of PQM-265 (**4c**).

Interestingly, the compound PQM-265 (**4c**) also showed non-concentration-dependent antioxidant effects with a considerable decrease of ROS formation at 2.5 µM. Similar behavior was observed for **4b**, which showed good activity against *t*-BuOOH in physiological—water medium, but with no significant activity against DPPH radical in ethanol solution. This suggests that the reaction environment conditions the ability of **4b** to counteract radical species.

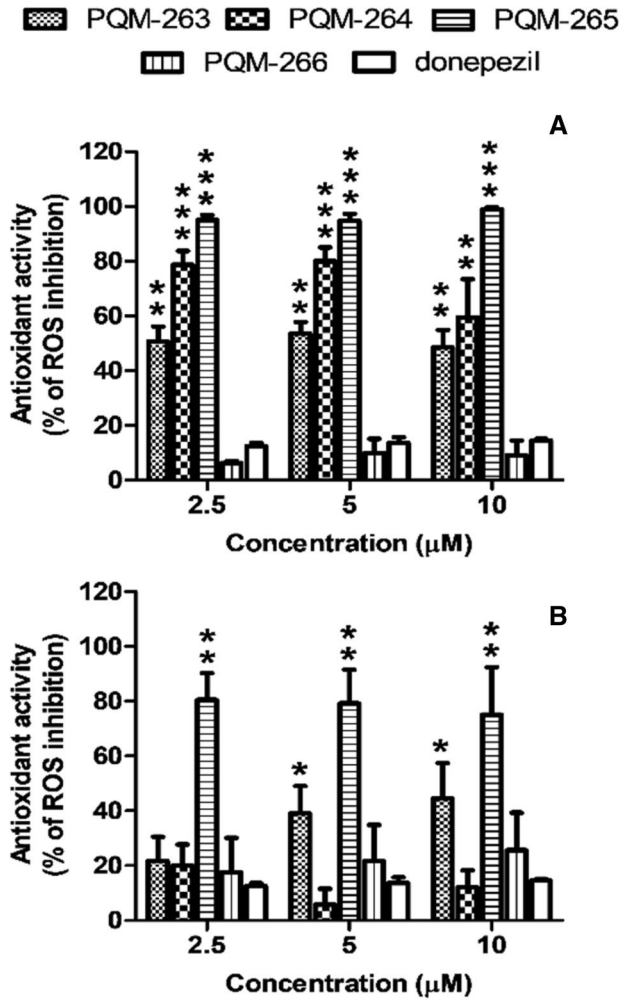

Fig. 5 Ability of compounds PQM-263 (**4a**), PQM-264 (**4b**), PQM-265 (**4c**) and PQM-266 (**4d**), to counteract (**a**, direct antioxidant activity) or prevent (**b**, indirect antioxidant activity) the intracellular ROS formation induced by *t*-BOOH in SH-SY5Y cells. **a** Cells were incubated with the studied compounds (2.5–10 μM) and *t*-BuOOH (100 μM) for 30 min; **b** Cells were incubated with the studied compounds (2.5–10 μM) for 24 h and then treated with *t*-BuOOH (100 μM) for 30 min. At the end of incubation, intracellular ROS formation was detected using the fluorescent probe H_2DCF-DA, as described in the experimental section. Data are expressed in terms of % of ROS inhibition and reported as mean ± SEM of three independent experiments (*p < 0.05, **p < 0.01 and ***p < 0.001 versus untreated cells at one-way ANOVA with Dunnett post hoc test)

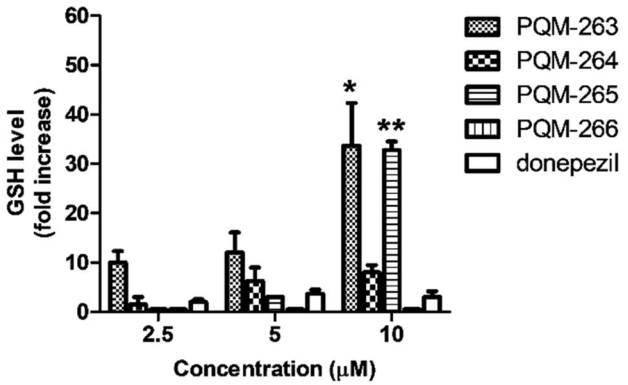

Fig. 6 Effects of compounds PQM-263 (**4a**), PQM-264 (**4b**), PQM-265 (**4c**) and PQM-266 (**4d**) on GSH levels in SH-SY5Y cells. Cells were incubated with the studied compounds (2.5–10 μM) for 24 h. At the end of incubation, GSH levels were detected using the fluorescent probe MCB, as described in the experimental section. Data are expressed as percentage increase of GSH and reported as mean ± SEM of three independent experiments (*p < 0.05 and **p < 0.01 versus untreated cells at one-way ANOVA with Dunnett post hoc test)

Finally, compound PQM-263 (**4a**), that showed the best effect in the DPPH test, also exhibited a significant antioxidant activity at neuronal cell level exposed to *t*-BuOOH using co-treatment test. These results reinforce our hypothesis that the ferulic acid pattern of compound **4a** positively contributes to neutralize the ROS formation and to protect the SH-SY5Y cell line from the oxidative damage. Then, the ability of these substances to prevent the formation of ROS induced by t-BuOOH was evaluated according to the pre-treatment approach. By this experimental approach, the cells are chronically treated with the test-compound for 24 h and then exposed to *t*-BuOOH for 30 min. In particular, by this approach it is possible to verify the ability of the compounds to enter into the cells and increase the endogenous antioxidant defenses (i.e. indirect antioxidant activity) [27]. As reported in Fig. 5b both PQM-263 (**4a**) and PQM-265 (**4c**) were capable to prevent the ROS formation, with the maximum indirect antioxidant activity of 44 and 75% at 10 μM, respectively.

By recording the reduction of ROS levels following a long treatment of the PQM-263 (**4a**) and PQM-265 (**4c**) before the treatment with *t*-BuOOH, we hypothesized that the antioxidant effect might likely result from an increase in levels of glutathione (GSH), an endogenous antioxidant for which key roles in protecting cells against oxidative stress damage have been recently demonstrated [28]. Thus, the intracellular GSH levels were analysed by employing the same experimental conditions used to evaluate the indirect antioxidant effect. Treatment of SH-SY5Y cells with PQM-263 (**4a**), PQM-264 (**4b**), PQM-265 (**4c**) and PQM-266 (**4d**) showed an increase in intracellular GSH levels at 10 μM only for **4a** (34%) and **4c** (33%) (Fig. 6).

These outcomes led us to choose compound **4a** and **4c** for further evaluation of its ability to activate Nrf2 binding to ARE at the nuclear level, an essential event for the induction of GSH production. The Nrf2 is the main regulator of phase II antioxidant response that is held in the cytosol by the repressor protein Kelch ECH associated protein 1 (Keap1) [27]. In the presence of oxidative stress, Nrf2 is released from keap1 and translocated into the nucleus, and

Table 6 ADMET predictions of the **4a-j** derivatives and the reference compound donepezil in the neutral form performed with the QikProp tool from Maestro

Compound	Ro5	MW	HBD[a]	HBA[a]	QPlogPo/w	HOA[b]	QPlogS	QPlogHERG	QPPMDCK
PQM-263 (**4a**)	0	379	3	4	3.9	87	− 5.2	− 7.6	55.7
PQM-264 (**4b**)	0	379	3	4	3.9	87	− 5.1	− 7.6	59.4
PQM-265 (**4c**)	0	365	4	4	3.0	74	− 4.5	− 7.5	18.0
PQM-266 (**4d**)	0	393	2	4	4.7	100	− 5.7	− 7.6	198.8
PQM-267 (**4e**)	0	363	2	3	4.6	100	− 5.4	− 7.7	199.0
PQM-268 (**4f**)	0	349	3	3	3.7	86	− 4.9	− 7.7	55.2
PQM-269 (**4 g**)	1	401	2	2	5.5	93	− 6.7	− 7.7	879.7
PQM-270 (**4 h**)	0	377	2	4	4.0	97	− 4.7	− 7.3	199.2
PQM-271 (**4i**)	1	368	2	2	5.0	90	− 6.0	− 7.7	492.6
PQM-272 (**4j**)	0	333	2	2	4.5	100	− 5.2	− 7.8	199.8
donepezil	0	379	1	3	4.1	100	− 4.2	− 6.4	439.6
Reference value	0–2	<500	≤ 5	≤ 10	≤ 5	> 80	− 6.5 - 0.5	> -5	> 500 great

[a]Properties obtained for the protonated state (pH 7.0)

[b]Given in percentage

once inside, it binds to the electrophile response element sequences to stimulate the expression of phase II antioxidant and anti-inflammatory genes [29]. The increased Nrf2 protein level in the cell nucleus by Keap1-dependent Nrf2 activation requires strong electrophiles disrupting of the Keap1-Nrf2 complex by modifying Keap1 at cysteine residues through the Michael reaction [30]. However, our results did not show the ability of both **4a** and **4c** in Nrf2 activation at 10 µM (data not shown). This result suggests that other mechanisms may be responsible for the induction of GSH expression, once the rate of glutathione biosynthesis is controlled by γ-glutamylcysteine synthetase, a typical cytoprotective enzyme that is upregulated by inducers coordinately with many other cytoprotective phase 2 genes [8].

Evaluation of Neuroprotective Activity Profile by Cell-Based Assay

The neuroprotective ability of compounds in DNs is generally linked with their antioxidant activity. The most important pathological mechanisms in the brain injury process include oxidative stress due to an imbalanced and excessive production of ROS that damage different cell structures, induce neuroinflammation and lead to neuronal death. To avoid the toxic effects of these reactive species, antioxidant compounds are thought to be used for controlling and neutralizing excessive free radicals and, in turn, protect different neuronal structures [31].

In Vitro Model of AD

Soluble $A\beta_{1\text{-}42}$ oligomers ($OA\beta_{1\text{-}42}$) are responsible for neurotoxic effects, among them neuronal cells death, and represents a key event in AD pathogenesis [32]. SH-SY5Y cells were incubated with $OA\beta_{1\text{-}42}$ (10 µM) and compounds **4a**, **4b** and **4c** (10 µM) for 4 h (Fig. 7a). Compound **4c**, but not **4a** and **4b**, significantly reduced $OA\beta_{1\text{-}42}$-induced neurotoxicity.

In Vitro Model of PD

The neurotoxin 6-hydroxydopamine (6-OHDA), by enhancing oxidative damage and neuroinflammation, provides an in vitro lesion model suitable for assessing the neuroprotective potential of PD therapeutics [33]. SH-SY5Y cells was treated with 6-OHDA (100 µM) and compounds **4a**, **4b** and **4c** (10 µM) for 2 h and starved in complete medium for 22 h (Fig. 7b). The results showed that compound **4a**, but not **4b** and **4c**, the ability to significantly counteract 6-OHDA-induced neurotoxicity.

In Vitro Model of HD

The neurotoxin 3-nitropropionic acid (3-NP) generates in animals behavioural, biochemical and morphologic changes similar to those occurring in HD, through several mechanisms including the irreversible inhibition of succinate dehydrogenase at mitochondrial level [34]. SH-SY5Y cells were incubated with 10 µM of PQM-263 (**4a**), PQM-264 (**4b**) and PQM-265 (**4c**) and 5 mM of 3-NP for 24 h (Fig. 7c). As in in vitro model of AD, only **4c** significantly reduced the neurotoxicity evoked by 3-NP.

The above results clearly underline a specific neuroprotective effect of **4a** against 6-OHDA insult suggesting a

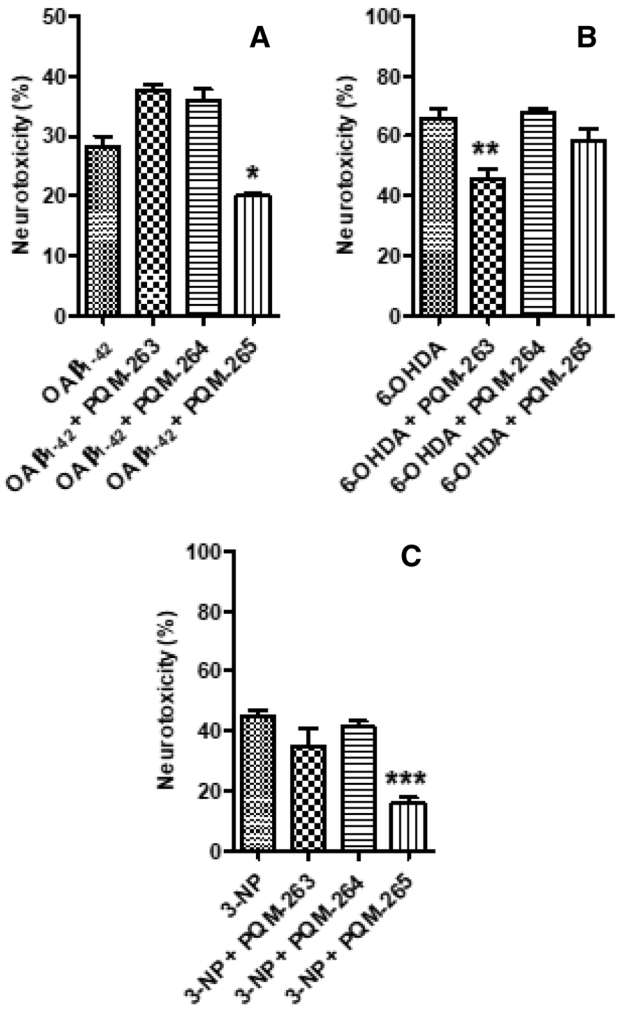

Fig. 7 Effects of compounds PQM-263 (**4a**), PQM-264 (**4b**) and PQM-265 (**4c**) on $OA\beta_{1\text{-}42}$, 6-OHDA and 3-NP induced neurotoxicity in SH-SY5Y cells. **a** Cells were incubated with compounds (10 μM) and $OA\beta_{1\text{-}42}$ (10 μ) for 4 h; **(B)** cells were incubated with compounds (10 μM) and 6-OHDA (100 μM) for 2 h and starved in complete medium for 22 h; **c** cells were incubated with compounds (10 μM) an3-NP (5 mM) for 24 h. The neurotoxicity was measured by MTT assay, as described in experimental section. Data are expressed as percentages of neurotoxicity versus cells treated with $OA\beta_{1\text{-}42}$ or 6-OHDA and reported as mean ± SEM of at least three independent experiments (* $p < 0.05$, ** $p < 0.01$ and *** $p < 0.001$ versus cells treated with neurotoxin at one-way ANOVA with Dunnett post hoc test)

potential usefulness as a promising ligand to prevent the oxidative stress in PD. Interestingly, **4c** show the ability to counteract the neurotoxicity induced by both $OA\beta_{1\text{-}42}$ and 3-NP, two neurotoxins that sharing the ability to induce mitochondrial dysfunction, a common mechanism in several neurodegenerative diseases. Therefore, both compound **4a** and **4c** could be explored as lead compound in pursuit of more effective molecules with multiple neuroprotective effects for DNs.

We evaluated the some relevant ADMET properties of the 4a-j derivatives and the reference compound donepezil in the neutral form through the QikProp tool from Maestro (Schrödinger Release 2018-4: QikProp, Schrödinger, LLC, New York, NY, 2018) (Table 6). The Lipinski's "Rule-of-five" (Ro5) comprises a set of molecular descriptors commonly used to evaluate the oral availability of small molecules: as: molecular weight (MW) ≤ 500 Da, lipophilicity assessed by the QPlogPo/w ≤ 5 (the predicted partition coefficient between octanol and water), number of hydrogen bond donors (HBD) and acceptors (HBA), respectively ≤ 5 and ≤ 10 [35]. We also evaluated the percentage of human oral absorption (HOA), water solubility (QPlogS), blockage of mammalian HERG K^+ channels (QPlogHERG), and permeability in Madin-Darby Canine Kidney (MDCK) cells (QPPMDCK). MDCK cells are considered to be a good mimic for the blood–brain barrier (BBB) and evaluates the BBB permeability for non-active transport. According to the QikProp predictions, all the compounds are drug-like molecules with no violations of the Ro5 rules (except compounds **4 g** and **4i** that slighly violate that ClogP criterion) with high human oral absorption (> 80%). For the most promising compounds (i.e., **4a** and **4d** as AChE inhibitors and **4j** as BuChE inhibitor), the ADMET predictions indicate that the BBB permeability and water solubility should be improved and the blockage mammalian HERG K^+ channels avoided in new derivatives of this class of compounds.

Among all ten synthetized compounds, most of them showed moderate inhibitory activity towards AChE or BuChE, with compound **4d** showing the best selective inhibition of AChE with $IC_{50} = 9.1$ μM. In addition, kinetic assays evidenced a mixed-type mechanism of inhibition for **4d** and showed a similar binding mode to that observed for donepezil. Considering the oxidative damage associated with NDs, all compounds were evaluated for their antioxidant activity, which results highlighted compound **4a** was the strongest antioxidant ligand, inhibiting 53.37% of DPPH radicals at 80 μM, followed by compound **4c** with 45.05% of inhibition at the same concentration. Moreover, the ability to inhibit the intracellular ROS formation induced by *t*-BOOH in SH-SY5Y cells corroborated the significant radical scavenging activity of **4a** and **4c**. The indirect antioxidant activity was determined through the ability of compounds **4a** and **4c** to induce glutathione release, showing an increase of 33 and 34% in the intracellular GSH levels, respectively. In vitro models of AD, PD and HD evidenced the neuroprotective effect of **4a** against 6-OHDA damage suggesting as a promising ligand to prevent the oxidative stress in PD. In addition, **4c** show the neuroprotective effect against mitochondrial dysfunction induced by both $OA\beta_{1\text{-}42}$ and 3-NP. Overall, considering the best multi-target profile of action of compounds **4a** and **4c**, being capable to selective inhibit AChE and

modulate neuronal oxidative damage, both ligands could be considered as promising lead compounds to be explored in pursuit of more effective molecules with multiple neuroprotective effects for DNs.

Experimental Section

NMR spectra of ^{1}H and ^{13}C were obtained on a Bruker AC-300 spectrometer operating at 300 MHz for ^{1}H NMR and 75 MHz for ^{13}C NMR in Nuclear Magnetic Resonance Laboratory at the Federal University of Alfenas (UNIFAL-MG). The samples were solubilized in DMSO-d_6 using TMS (tetramethylsilane) as the internal reference. Infrared (IR) spectra have been generated in an infrared spectrometer Thermo Scientific USA (Nicolet iS50 model) coupled to Pike Gladi ATR technologies in analysis and characterization of drugs laboratory (LACFar) at the UNIFAL-MG. Mass spectrometric analyzes were acquired in a range of *m/z* of 80–1000 in the BRUKER COMPASS mass spectrometer by electrospray ionization. The purity of compounds was determined by High Performance Liquid Chromatography (HPLC) Shimadzu. Thin layer chromatography experiments were performed on silica gel sheet 60 F254, Merck and purification by chromatography column was performed on flash silica gel (220–440 mesh, 0.035 mm–0.075 mm), Sigma-Aldrich. The visualization of the substances was done in UV chamber (λ = 254 or 365 nm). Melting point were made on Mars equipment (PFM II) with crushed sample and packaged in capillary tube. All spectra are available in the supplementary material.

General Procedure for the Synthesis of Hydrazide Intermediates 6a-j

To a suspension of *trans*-cinnamic acid derivatives **5a-j** (1 eq 1.51 mmol) in 15 mL of acetonitrile at room temperature, was added 1.2 eq. (1.81 mmol) of HOBT and 1.2 eq. (1.81 mmol) of EDC. The reaction was stirred for 2 hat room temperature (25 °C). The resulting mixture was then slowly added to a solution of hydrazine hydrate (10 eq.) in 10 mL of acetonitrile and stirred in a second ice-bath flask, kept between 0 and 10 °C. Then, the solvent was removed under low pressure and dried under vacuum. Finally, the resultant solid was re-suspended in 4 mL of 5% saturated $NaHCO_3$ and stirred to allow formation of the precipitate. The solid was separated by filtration and washed with cold water to obtain the hydrazide intermediates **6a-j.**

(E)-3-(4-hydroxy-3-methylphenyl)acrylohydrazide (**6a**). Yield 96%, white solid. IR (ATR): ν 3401, 3306, 3143, 2945, 1656, 1580, 1514, 1278 and 1043 cm^{-1}. ^{1}H NMR (300 MHz, DMSO-d_6) δ 9.16 (s, 2H, CONHNH$_2$), 7.32 (d, J = 15.75 Hz, 1H, HC = CH), 7.09 (d, J = 1.89 Hz, 1H, Ar–H), 6.97 (dd, J = 1.89, 8.13 Hz, 1H, Ar–H), 6.77 (d, J = 8.13 Hz, 1H, Ar–H), 6.34 (d, J = 15.75 Hz, 1H, HC = CH), 4.37 (s, 2H, CONHNH$_2$) and 3.78 (s, 3H, CH$_3$). ^{13}C NMR (75 MHz, DMSO-d_6) δ 165.3, 148.7, 148.3, 139.1, 126.9, 121.8, 117.4, 116.1, 111.3 and 56.0.

(E)-3-(3-hydroxy-4-methoxyphenyl)acrylohydrazide (**6b**). Yield 78%, white solid. IR (ATR): ν 3334, 1650, 1598 and 1494 cm^{-1}. ^{1}H NMR (300 MHz, DMSO-d_6) δ 9.24 (s, 2H, CONHNH$_2$), 9.19 (s, 1H, OH), 7.30 (d, J = 15.74 Hz, 1H, HC = CH), 6.99 (d, J = 1.56 Hz, 1H, Ar–H), 6.95-6.93 (m, 1H, Ar–H), 6.93 (d, J = 8.13 Hz, 1H, Ar–H), 6.32 (d, J = 15.74 Hz, 1H, HC = CH), 4.42 (s, 2H, CONHNH$_2$) and 3.79 (s, 3H, CH$_3$). ^{13}C NMR (75 MHz, DMSO-d_6) δ 164.7, 148.9, 146.5, 138.1, 127.6, 120.0, 117.3, 113.2, 111.9 and 55.4.

(E)-3-(3,4-dihydroxyphenyl)acrylohydrazide (**6c**). Yield 38%, Yellow solid. IR (ATR): ν 3443, 3340, 3264, 3027, 1686, 1639, 1591 and 1524 cm^{-1}. ^{1}H NMR (300 MHz, DMSO-d_6) δ 9.24 (s, 2H, CONHNH$_2$), 7.27 (d, J = 15.72 Hz, 1H, HC = CH), 6.95 (d, J = 1.96 Hz, 1H, Ar–H), 6.84 (dd, J = 1.96, 8.10 Hz, 1H, Ar–H), 6.74 (d, J = 8.10 Hz, 1H, Ar–H), 6.26 (d, J = 15.72 Hz, 1H, HC = CH) and 4.43 (s, 2H, CONHNH$_2$). ^{13}C NMR (75 MHz, DMSO-d_6) δ 165.6, 147.8, 146.0, 139.2, 126.8, 120.9, 116.9, 116.2 and 114.0.

(E)-3-(3,4-dimethoxyphenyl)acrylohydrazide (**6d**). Yield 84%, white solid. IR (ATR): ν 3231, 3034, 2962, 1652, 1616, 1582, 1510 and 1263 cm^{-1}. ^{1}H NMR (300 MHz, DMSO-d_6) δ 9.19 (s, 2H, CONHNH$_2$), 7.37 (d, J = 15.77 Hz, 1H, HC = CH), 7.12 (d, J = 1.84 Hz, 1H, Ar–H), 6.97 (dd, J = 1.84, 8.25 Hz, 1H, Ar–H), 6.95 (d, J = 8.25 Hz, 1H, Ar–H), 7.09 (d, J = 15.77 Hz, 1H, HC = CH), 4.39 (s, 2H, CONHNH$_2$), 3.78 (s, 3H, CH$_3$) and 3.76 (s, 3H, CH$_3$). ^{13}C NMR (75 MHz, DMSO-d_6) δ 164.8, 150.0, 148.8, 138.2, 127.6, 121.1, 117.8, 111.7, 110.0 and 55.5.

(E)-3-(4-methoxyphenyl)acrylohydrazide (**6e**). Yield 58%, white solid. IR (ATR): ν 3278, 3013, 1655, 1600 and 1507 cm^{-1}. ^{1}H NMR (300 MHz, DMSO-d_6) δ 9.26 (s, 2H, CONHNH$_2$), 7.47 (d, J = 8.57 Hz, 2H, Ar–H), 7.37 (d, J = 15.80 Hz, 1H, HC = CH), 6.94 (d, J = 8.57 Hz, 2H, Ar–H), 6.38 (d, J = 15.80 Hz, 1H, HC = CH), 4.45 (s, 2H, CONHNH$_2$) and 3.75 (s, 3H, CH$_3$). ^{13}C NMR (75 MHz, DMSO-d_6) δ 165.4, 160.7, 138.3, 129.5, 127.9, 118.2, 114.8 and 55.7.

(E)-3-(4-hydroxyphenyl)acrylohydrazide (**6f**). Yield 79%, Light yelow solid. IR (ATR): ν 3269, 3195, 3013, 2906, 1632, 1606, 1587 and 1511 cm^{-1}. ^{1}H NMR (300 MHz, DMSO-d_6) δ 9.18 (s, 2H, CONHNH$_2$), 7.36 (d, J = 8.58 Hz, 2H, Ar–H), 7.33 (d, J = 15.81 Hz, 1H, HC = CH), 6.77 (d, J = 8.58 Hz, 2H, Ar–H), 6.31 (d, J = 15.81 Hz, 1H, HC = CH) and 4.36 (s, 2H, CONHNH$_2$). ^{13}C NMR (75 MHz, DMSO-d_6) δ 165.6, 159.3, 138.8, 129.8, 126.4, 117.1 and 116.2.

(E)-3-(4-(trifluoromethyl)phenyl)acrylohydrazide (**6 g**). Yield 76%, white solid. IR (ATR): ν 3317, 3219, 3028, 1649, 1609 and 1528 cm^{-1}. ^1H NMR (300 MHz, DMSO-d_6) δ 9.45 (s, 2H, CONHNH$_2$), 7.77-7.70 (m, 4H, Ar–H), 6.66 (d, *J* = 15.87 Hz, 1H, HC = CH) and 4.49 (s, 2H, CONHNH$_2$). ^{13}C NMR (75 MHz, DMSO-d_6) δ 164.2, 139.5, 136.9, 129.6 (d, *J* = 31.88 Hz), 128.5, 126.2 (d, *J* = 3.53 Hz), 124.6 (d, *J* = 271.85 Hz) and 123.6.

(E)-3-(benzo[d] [1, 3] dioxol-5-yl)acrylohydrazide (**6 h**). Yield 66%, Light brown solid. IR (ATR): ν 3342, 3191, 3031, 1660, 1625, 1552 and 1493 cm^{-1}. ^1H NMR (300 MHz, DMSO-d_6) δ 9.21 (s, 2H, CONHNH$_2$), 7.34 (d, *J* = 15.76 Hz, 1H, HC = CH), 7.04 (dd, *J* = 1.50, 8.01 Hz, 1H, Ar–H), 7.10 (d, *J* = 1.50 Hz, 1H, Ar–H), 6.91 (d, *J* = 8.01 Hz, 1H, Ar–H), 6.03 (s, 2H, CH_2), 6.36 (d, *J* = 15.76 Hz, 1H, HC = CH) and 4.39 (s, 2H, CONHNH$_2$). ^{13}C NMR (75 MHz, DMSO-d_6) δ 165.2, 148.9, 148.4, 138.5, 129.8, 123.5, 118.8, 109.0, 106.6 and 101.9.

(E)-3-(4-chlorophenyl)acrylohydrazide (**6i**). Yield 82%, white solid. IR (ATR): ν 3311, 3247, 3032, 1650, 1608, 1519 and 1036 cm^{-1}. ^1H NMR (300 MHz, DMSO-d_6) δ 9.40 (s, 2H, CONHNH$_2$), 7.58 (d, *J* = 8.53 Hz, 2H, Ar–H), 7.46 (d, *J* = 8.53 Hz, 2H, Ar–H), 7.43 (d, *J* = 15.87 Hz, 1H, HC = CH), 6.54 (d, *J* = 15.87 Hz, 1H, HC = CH) and 4.49 (s, 2H, CONHNH$_2$). ^{13}C NMR (75 MHz, DMSO-d_6) δ 164.7, 137.3, 134.3, 134.3, 129.6, 129.4 and 121.5.

Cinnamoylhydrazide (**6j**). Yield 28%, Light yellow solid. IR (ATR): ν 3285, 3025, 1651, 1612 and 1522 cm^{-1}. ^1H NMR (300 MHz, DMSO-d_6) δ 9.36 (s, 2H, CONHNH$_2$), 7.54 (d, *J* = 6.73 Hz, 2H, Ar–H), 7.43 (d, *J* = 15.84 Hz, 1H, HC = CH), 7.40-7.31 (m, 3H, Ar–H), 6.54 (d, *J* = 15.84 Hz, 1H, HC = CH) and 4.46 (s, 2H, CONHNH$_2$). ^{13}C NMR (75 MHz, DMSO-d_6) δ 164.9, 138.6, 135.4, 129.9, 129.4, 127.9 and 120.7.

*General procedure for the coupling reaction between the hydrazide intermediates **6a-j** with 1-benzyl-4-piperidone for the preparation of compounds **4a-j***

To a solution 1.2 eq of 1-benzyl-4-piperidone in 10 mL of ethanol, was added 0.96 mmol of the corresponding hydrazide intermediates **6a-j**. The mixture was stirred at room temperature until total consumption of the corresponding hydrazide visualized by TLC using a mixture of hexane/ethyl acetate (3: 7) as eluent. Then, the solvent was removed under reduced pressure and the product was purified by flash chromatography column (CC) and a mixtures of hexane/Ethyl acetate in gradient concentration or by recrystallization from ethanol/dichloromethane.

(E)-N'-(1-benzylpiperidin-4-ylidene)-3-(4-hydroxy-3-methoxyphenyl)acrylohydrazide (**4a**). White solid (yield 46%), m.p. 203 °C. IR (ATR): ν 3330, 3029, 2945, 1682, 1628, 1588 and 1530 cm^{-1}. ^1H NMR (300 MHz, DMSO- d_6) δ 10.36 and 10.33 (s, 1H, NH), 9.51 (s, 2H, OH), 7.39-7.25 (m, 8H, Ar–H), 7.30-7.23 (m, 2H, Ar–H), 7.53 and 7.45 (d, *J* = 16.5 and 15.6 Hz, 1H, HC = CH), 7.17 and 7.08 (d, *J* = 8.0 and 7.9 Hz, 1H, Ar–H), 7.17 and 7.03 (d, *J* = 8.0 and 7.9 Hz, 1H, Ar–H), 6.81 (d, *J* = 7.9 Hz, 2H, Ar–H),6.66 (d, *J* = 8.1 Hz, 1H, HC = CH), 3.81 (s, 6H, OCH_3), 3.54 (s, 4H, CH_2) and 2.37 (t, *J* = 5.3 Hz, 2H, CH_2). ^{13}C NMR (75 MHz, DMSO-d_6) δ 162.0, 157.3, 152.1, 148.7, 148.4, 147.7, 142.0, 140.2, 138.2, 128.6, 128.1, 126.9, 126.3, 121.8, 117.2, 115.6, 114.2, 111.4, 110.6, 61.3, 55.4, 53.2, 51.8, 34.2 and 27.2. HR-MS (ESI) *m/z*: Calcd for $C_{22}H_{25}N_3O_3$ $[M+H]^+$: 380.1974, found: 380.1978.

E)-N'-(1-benzylpiperidin-4-ylidene)-3-(3-hydroxy-4-methoxyphenyl)acrylohydrazide (**4b**). White solid (yield 37%), m.p. 192 °C. IR (ATR): ν 3246, 3026, 2901, 1659, 1646 and 1586 cm^{-1}. ^1H NMR (300 MHz, DMSO- d_6) δ 10.39 and 10.36 (s, 1H, NH), 9.22 (s, 2H, OH), 7.48 and 7.39 (d, *J* = 15.7 and 15.6 Hz, 1H, HC = CH), 7.34 (d, *J* = 4.4 Hz, 8H, Ar–H), 7.31-7.22 (m, 2H, Ar–H), 7.28 and 6.61 (d, *J* = 15.7 and 15.6 Hz, 1H, HC = CH), 7.09 and 7.02 (s, 1H, Ar–H), 7.01 and 6.98 (d, *J* = 8.4 and 7.8 Hz, 1H, Ar–H), 6.95 (d, *J* = 7.8 Hz, 2H, Ar–H), 3.80 (s, 6H, OCH_3), 3.54 (s, 4H, CH_2) and 2.36 (t, *J* = 5.5 Hz, 2H, CH_2). ^{13}C NMR (75 MHz, DMSO-d_6) δ 166.7, 162.0, 157.7, 152.5, 149.6, 149.4 146.8, 141.8, 140.1, 137.9, 128.8, 128.3, 127.9, 127.0, 121.1, 120.5, 118.1, 115.0, 113.5, 112.1, 61.4, 55.7, 53.28, 52.0, 34.4 and 27.4. HR-MS (ESI) *m/z*: Calcd for $C_{22}H_{25}N_3O_3$ $[M+H]^+$: 380.1974, found: 380.1978.

(E)-N'-(1-benzylpiperidin-4-ylidene)-3-(3,4-dihydroxyphenyl)acrylohydrazide (**4c**). Yellow solid (yield 19%), m.p. 140 °C. IR (ATR): ν 3243, 2796, 1650, 1597, 1535 and 1516 cm^{-1}. ^1H NMR (300 MHz, DMSO- d_6) δ 10.32 (s, 2H, NH), 9.24 (s, 2H, OH), 7.42 and 7.36 (d, *J* = 15.4 and 15.6 Hz, 1H, HC = CH), 7.34-7.27 (m, 8H, Ar–H), 7.17 and 6.65 (d, *J* = 15.4 and 15.6 Hz, 1H, HC = CH), 7.03 and 6.96 (s, 1H, Ar–H), 6.90 and 6.85 (d, *J* = 7.0 and 8.2 Hz, 1H, Ar–H), 6.74 (d, *J* = 8.2 Hz, 2H, Ar–H), 3.51 (s, 4H, CH_2) and 2.33 (t, *J* = 5.3 Hz, 2H, CH_2) ^{13}C NMR (75 MHz, DMSO-d_6) δ 166.7, 162.0, 157.3, 152.2, 147.7, 147.5, 145.5, 142.0, 138.2, 128.6, 128.1, 126.9, 126.3, 121.1, 120.5, 116.8, 115.7, 113.8, 113.8, 61.2, 53.1, 51.8, 34.2 and 27.2. HR-MS (ESI) *m/z*: Calcd for $C_{21}H_{23}N_3O_3$ $[M+H]^+$: 366.1818, found: 366.1803.

(E)-N'-(1-benzylpiperidin-4-ylidene)-3-(3,4-dimethoxyphenyl)acrylohydrazide (**4d**). White solid (yield 55%), m.p. 185 °C. IR (ATR): ν 3231, 3034, 2795, 1652, 1616, 1536 and 1510 cm^{-1}. ^1H NMR (300 MHz, DMSO- d_6) δ 10.36 (s, 2H, NH), 7.55 and 7.46 (d, *J* = 15.6 and 15.5 Hz, 1H, HC = CH), 7.33–7.30 (m, 8H, Ar–H), 7.27-7.19 (m, 2H, Ar–H), 7.30 and 6.70 (d, *J* = 15.6 and 15.5 Hz, 1H, HC = CH), 7.20 and 7.15 (s, 1H, Ar–H), 7.13 (d, *J* = 8.0 Hz, 1H, Ar–H), 6.97 (d, *J* = 8.0 Hz, 2H, Ar–H), 3.78 (s, 6H, OCH_3), 3.76 (s, 6H, OCH_3), 3.51 (s, 4H, CH_2) and 2.38-2.31 (m, 2H, CH_2). ^{13}C NMR (75 MHz, DMSO-d_6) δ 166.4, 161.6, 157.2, 152.1, 150.2,150.0, 148.6, 141.5, 139.6, 138.1,

128.4, 127.9, 127.4, 126.7, 121.6, 121.3, 118.0, 115.0, 111.5, 110.4, 109.6, 61.0, 55.3, 55.3, 53.0, 51.6, 34.0 and 27.0.HR-MS (ESI) *m/z*: Calcd for $C_{23}H_{27}N_3O_3$ $[M+H]^+$: 394.2131, found: 394.2124.

(E)-N'-(1-benzylpiperidin-4-ylidene)-3-(4-methoxyphenyl)acrylohydrazide (**4e**). White solid (yield 29%), m.p. > 300 °C. IR (ATR): ν 3096, 1655, 1625, 1542 and 1511 cm^{-1}. ^1H NMR (300 MHz, DMSO- d_6) δ 10.45 and 10.41 (s, 2H, NH), 7.60 and 7.54 (d, *J* = 8.3 and 8.7 Hz, 8H, Ar–H), 7.55 and 7.49 (d, *J* = 15.7 and 15.5 Hz, 1H, HC = CH), 7.34 (d, *J* = 4.3 Hz, 8H, Ar–H), 7.30-7.23 (m, 2H, Ar–H), 7.28 and 6.73 (d, *J* = 15.7 and 15.5 Hz, 1H, HC = CH), 6.99 (d, *J* = 8.7 Hz, 4H, Ar–H), 3.79 (s, 6H, OCH_3), 3.53 (s, 4H, CH_2) and 2.36 (t, *J* = 5.4 Hz, 2H, CH_2). ^{13}C NMR (75 MHz, DMSO-d_6) δ 167.1, 162.4, 161.1, 160.9, 158.1, 153.0, 141.8, 140.0, 138.8, 130.2, 130.2, 129.2, 128.7, 128.0, 127.5, 118.7, 115.6, 114.9, 114.9, 61.8, 55.7, 53.7, 52.4, 34.4 and 27.4. HR-MS (ESI) *m/z*: Calcd for $C_{22}H_{25}N_3O_2$ $[M+H]^+$: 364.2025, found: 364.2014.

(E)-N'-(1-benzylpiperidin-4-ylidene)-3-(4-hydroxyphenyl)acrylohydrazide (**4f**). Yellow solid (yield 39%), m.p. 223 °C. IR (ATR): ν 3215, 2812, 1650, 1598, 1550 and 1514 cm^{-1}. ^1H NMR (300 MHz, DMSO- d_6) δ 10.34 and 10.30 (s, 2H, NH), 9.90 (s,1H, OH), 7.50 and 7.41 (d, *J* = 16.4 and 15.6 Hz, 1H, HC = CH), 7.40 (d, *J* = 7.8 Hz, 4H, Ar–H), 7.31 (d, *J* = 4.2 Hz, 8H, Ar–H), 7.28-7.21 (m, 2H, Ar–H), 7.23 and 6.61 (d, *J* = 16.4 and 15.6 Hz, 1H, HC = CH), 6.78 (d, *J* = 7.8 Hz, 4H, Ar–H), 3.51 (s, 4H, CH_2) and 2.36-2.31 (m, 2H, CH_2). ^{13}C NMR (75 MHz, DMSO-d_6) δ 166.7, 162.0, 159.2, 158.9, 157.4, 152.2, 141.6, 139.9, 138.2, 129.3, 129.3, 128.6, 128.1, 126.9, 125.9, 117.0, 115.7, 115.7, 113.9, 61.2, 53.1, 51.8, 34.2 and 27.2. HR-MS (ESI) *m/z*: Calcd for $C_{21}H_{23}N_3O_2$ $[M+H]^+$: 350.1869, found: 350.1858.

(E)-N'-(1-benzylpiperidin-4-ylidene)-3-(4-(trifluoromethyl)phenyl)acrylohydrazide (**4 g**). White solid (yield 57%), m.p. 188 °C. IR (ATR): ν 3243, 3027, 1649, 1609 and 1528 cm^{-1}. ^1H NMR (300 MHz, Pyridine-d_5) δ 10.61 and 10.56 (s, 2H, NH), 8.14 and 8.06 (d, *J* = 16.0 and 15.7 Hz, 1H, HC = CH), 7.71 (d, *J* = 8.1 Hz, 4H, Ar–H), 7.60 (d, *J* = 8.1 Hz, 4H, Ar–H), 7.45-7.27 (m, 10H, Ar–H), 7.38 and 7.05 (d, *J* = 16.0 and 15.7 Hz, 1H, HC = CH), 3.48 (s, 4H, CH_2) and 2.85–2.42 (m, 16H, CH_2). ^{13}C NMR (75 MHz, DMSO-d_6) δ 166.40 161.5, 159.1, 153.8, 140.1, 139.4, 138.5, 130.0, 129.2, 129.1, 128.7, 127.5, 126.4, 126.4, 124.2, 122.8, 121.2, 61.7, 53.7, 52.4, 34.8 and 27.9. HR-MS (ESI) *m/z*: Calcd for $C_{22}H_{22}FN_3O$ $[M+H]^+$: 402.1793, found: 402.1783.

(E)-3-(benzo[d] [1, 3] dioxol-5-yl)-N'-(1-benzylpiperidin-4-ylidene)acrylohydrazide (**4 h**). Light brown solid (yield 56%), m.p. 90 °C. IR (ATR): ν 3220, 3024, 2949, 1656, 1600, 1527 and 1488 cm^{-1}. ^1H NMR (300 MHz, DMSO- d_6) δ 10.39 (s, 2H, NH), 7.51 and 7.43 (d, *J* = 15.9 and 15.7 Hz, 1H, HC = CH), 7.25 and 7.12 (s, 2H, Ar–H), 7.32 (d, *J* = 4.3 Hz, 8H, Ar–H),), 7.32 and 6.67 (d, *J* = 15.9 and 15.7 Hz, 1H, HC = CH), 7.28-7.21 (m, 2H, Ar–H), 7.13 and 7.09 (d, *J* = 8.1 Hz, 4H, Ar–H), 6.94 (d, *J* = 8.1 Hz, 2H, Ar–H), 6.05 (s, 4H, CH_2), 3.52 (s, 4H, CH_2) and 2.34 (t, *J* = 5.1 Hz 2H, CH_2). ^{13}C NMR (75 MHz, DMSO-d_6) δ 167.1, 162.3, 158.2, 153.0, 149.1, 148.4, 148.3, 141.8, 140.1, 138.8, 129.8, 129.2, 128.7, 127.5, 124.4, 123.9, 119.2, 116.3, 109.1, 107.2, 106.6, 102.0, 61.8, 53.7, 52.4, 34.7 and 27.8. HR-MS (ESI) *m/z*: Calcd for $C_{22}H_{23}N_3O_3$ $[M+H]^+$: 378.1818, found: 378.1801.

(E)-N'-(1-benzylpiperidin-4-ylidene)-3-(4-chlorophenyl) acrylohydrazide (**4i**). White solid (yield 73%), m.p. 209 °C. IR (ATR): ν 3164, 3051, 2905, 1662, 1615 and 1490 cm^{-1}. ^1H 9NMR (300 MHz, DMSO- d_6) δ 10.51 and 10.34 (s, 2H, NH), 7.68-7.59 (m, 4H, Ar–H), 7.54 and 7.49 (d, *J* = 16.7 and 15.7 Hz, 1H, HC = CH), 7.49-7.44 (m, 4H, Ar–H), 7.31 (d, *J* = 4.3 Hz, 8H, Ar–H), 7.28-7.20 (m, 2H, Ar–H), 7.27 and 6.81 (d, *J* = 16.7 and 15.7 Hz, 1H, HC = CH) and 2.49-2.47 (m, 2H, CH_2). ^{13}C NMR (75 MHz, DMSO-d_6) δ 161.9, 159.2, 139.0, 138.6, 134.6, 134.3, 129.8, 129.8, 129.5, 129.3, 128.7, 127.5, 121.9, 61.7, 53.6, 52.3, 34.6 and 27.8. HR-MS (ESI) *m/z*: Calcd for $C_{21}H_{22}ClN_3O$ $[M+H]^+$: 368.1530, found: 368.1525.

N'-(1-benzylpiperidin-4-ylidene)cinnamohydrazide (**4j**). Light yellow solid (yield 11%), m.p. 183 °C. IR (ATR): ν 3231, 3028, 2790, 1673, 1655, 1538 and 1494 cm^{-1}. 10.48 (s, 2H, NH), 7.62 and 7.55 (d, *J* = 15.6 and 15.7 Hz, 1H, HC = CH), 7.59 (d, *J* = 6.7 Hz, 4H, Ar–H), 7.45-7.40 (m, 2H, Ar–H), 7.42 (d, *J* = 6.7 Hz, 4H, Ar–H), 7.33 (d, *J* = 3.5 Hz, 8H, Ar–H), 7.30-7.23 (m, 2H, Ar–H), 7.43 and 6.87 (d, *J* = 15.6 and 15.7 Hz, 1H, HC = CH), 3.54 (s, 4H, CH_2) and 2.40-2.36 (m, 2H, CH_2). ^{13}C NMR (75 MHz, DMSO-d_6) δ 166.8, 162.0, 158.7, 153.7, 141.9, 140.2, 138.8, 130.8, 130.3, 130.1, 129.4, 129.2, 128.7, 128.1, 127.4, 121.3, 118.3, 61.7, 53.7, 52.4, 34.8 and 27.9. HR-MS (ESI) *m/z*: Calcd for $C_{21}H_{23}N_3O$ $[M+H]^+$: 334.1919, found: 334.1919.

Molecular Docking Study with AChE

In this work, we evaluated the possible binding modes of the compounds 4a-4j against the AChE through the molecular docking strategy. Due to the similarity of the derivatives synthesized in this work with donepezil, we performed the docking experiments in the structure 4EY7 (human AChE solved at 2.35 Å in complex with donepezil) [36]. Conserved waters were identified through the superposition of the AChE structures and considered explicitly during the docking experiments [37]. The four water molecules W729, W722, W731 and W737 were

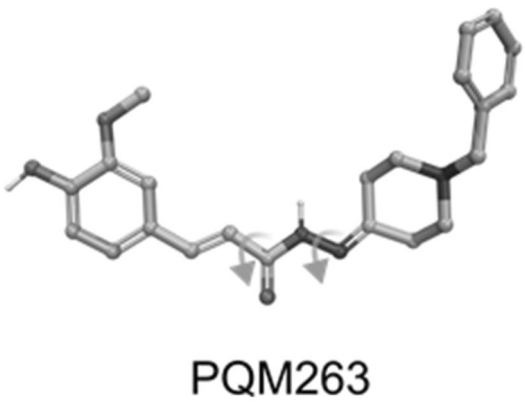

Fig. 8 Rotatable bonds kept fixed during the docking experiments as highlighted as arrows. Dihedrals not highlighted in this picture were defined as free to rotate, except amide bonds

extracted from the structure of the AChE complexed with donepezil (PDB code 4EY7). For BuChE, we used the recently solved structure complexed with a large chlorotacrine-based inhibitor (PDB code 6I0C, solved at 2.65 Å) [38]. The receptor structures were prepared with Protein Preparation Wizard tool from the Schrödinger Suite 2018-4 [39] and the protonation states of the amino acid residues were predicted using PROPKA with pH = 7. Finally, the optimization of the hydrogen bond network of the protein–ligand complexes was performed to adjust the orientation of the hydrogen atoms, followed by energy minimization of the hydrogen atoms.

The compounds were designed and prepared with LigPrep from Maestro to set up the isomers, protonation states and tautomers with Epik [40] at pH 7.0 ± 0.4. We applied torsional constraints to some rotatable bonds to keep the planarity observed for the compounds during the docking experiments (Fig. 8). The rotatable bond from the amide group was kept fixed to the trans conformation.

The docking experiments were performed with the molecular docking program Glide from Maestro in the SP precision mode [41]. All the AChE structures and the BuChE structure were aligned to the 1ZGC conformation using the *super* tool from Pymol. The receptor grids were centred on the native ligand present in the aligned 1Q84 complex, which contains a large inhibitor at both CAS and PAS binding sites (X: 98.06, Y: 53.14 and Z: 22.06). We also redocked the co-crystallized ligands into their respective structures to validate the docking protocol. The top-energy docked pose of each ligand was selected according to the lowest Glide Emodel. The predicted binding affinity was provided as the "docking score", consisting of the GlideScore and the Epik penalization due to the selected protonation state.

Anti-cholinesterase Activity Assays

Anticholinesterase activity was determined according to Ellman's method [15] modified for 96-well plates as previously described [42]. All solutions were prepared in tris–HCl buffer (0.02 M, pH 7.5) and stock solutions of the test compounds were prepared in DMSO (50 mM). In 96-well plates were added solutions with the inhibitor compound at 30 µM final concentration. The vehicle control (DMSO-final concentration 0.2% v/v for AChE) was used as reference (negative control) and the reagent 5,5′-Dithiobis-2-nitrobenzoic acid (DTNB) was added to electric eel acetylcholinesterase (*Ee*AChE) or equine serum butyrylcholinesterase (*Eq*BuChE) in presence of bovine serum albumin (BSA). Absorbance was recorded using an iMark plate reader (Bio-Rad) equipped with a light filter of = 415 nm and this measurement used as a blank reference. After 10 min incubation at room temperature, acetylthiocholine iodide (ACTI) or *S*-butyrylthiocholine iodide (BCTI) was added and absorbance was recorded after 10 min of incubation at room temperature at λ = 415 nm for 3 times within 30 s. Enzyme activity was calculated as a percentage of the mean absorbance values measured for the DMSO-treated control, discounted from the mean blank reference values. Assays were performed in triplicate (for standard deviation calculation). Inhibition values were calculated using the Excel program.

Enzyme Kinetic Assay

Enzymatic kinetic was determined according to Ellman's method [15] modified for 96-well plates as previously described [42, 43]. All solutions were prepared in tris–HCl buffer (0.02 M, pH 7.5) and the stock solutions of the test compounds were prepared in DMSO (2 mM). In 96-well plates were added 150 µL inhibitor compound solution of compound **4j** at two different concentrations (10 and 13 µM) distributed in eight sets of triplicates each. Eight sets of DMSO-treated untreated triplicates (final concentration 0.18% v/v of BuChE) were used as negative control. Subsequently, was added 60 µL of DTNB (Ellman's reagent) to 1.1 mM and 30 µL of equine serum butyrylcholinesterase (*Eq*BChE) at 0.20 U/mL in the presence of 1 mg/mL bovine serum albumin (BSA). Absorbance was then recorded using an iMark plate reader (Bio-Rad) equipped with λ = 415 nm light filter and this measurement used as a blank reference. After 10 min incubation at 25 °C, 24 µL of substrate (BCTI) at eight serially diluted concentrations (factor = 1.3) of 2.75–0 44 mM (final concentration: 0.25–0.04 mM) were added to the respective wells and the absorbance recorded after incubation for 10 min at 25 °C at λ = 415 nm. The Lineweaver–Burk

reciprocal plots were obtained by plotting a 1/velocity *versus* 1/[substrate] and two different inhibitor concentrations for untreated control. The linear regression of each data-set shows a convergent behavior, in ways the region to where the curves converge determine the type of inhibition. The values of K_i, $K_{i'}$ (competitive and non-competitive inhibition constants respectively), K_m (Michaelis–Menten constant) and V_{max} (maximum speed) were calculated using Graphpad Prism 7.0 using nonlinear regression models for kinetics. enzymatic - inhibition and enzymatic kinetics-substrate *versus* velocity.

DPPH Scavenging Activity

The ability of compounds PQM 263–272 to scavenge DPPH free radicals was evaluated according to the method described by Gontijo 2012 [44] in our laboratory (PeQuiM). The compounds were evaluated at concentrations of 200, 100, 50, 25, 12.5, 6.25, 3.13 and 1.56 µM in ethanol. A 4 mL aliquot of sample was mixed with 1 mL of DPPH (0.5 mM in ethanol). The solution was vigorously stirred at room temperature and after 30 min the absorbance was measured at 517 nm in a UV–vis spectrophotometer (Shimadzu). A low absorbance value indicates effective free radical scavenging. Each solution was analyzed in triplicate and the mean values were plotted to obtain the EC_{50} against DPPH by linear regression. Antioxidants like ascorbic acid and trolox were used as a standard over the same range of concentrations. The radical-scavenging activity was evaluated as the percentage of inhibition according to the following equation: %inhibition = [(absorbance of control − absorbance of sample)/absorbance of control)] × 100.

Determination of Neurotoxicity

Human neuronal (SH-SY5Y) cells were routinely grown in Dulbecco's modified Eagle's Medium supplemented with 10% fetal bovine serum, 2 mM L-glutamine, 50 U/mL penicillin and 50 µg/mL streptomycin at 37 °C in a humidified incubator with 5% CO_2.

Cells viability, in terms of mitochondrial metabolic function, was evaluated by the reduction of 3-(4,5-dimethyl-2-thiazolyl)-2,5-diphenyl-2H-tetrazolium bromide (MTT) to its insoluble formazan, as previously described [45]. SH-SY5Y cells were seeded in a 96-well plate at 2×10^4 cells/well, incubated for 24 h and subsequently treated with different concentrations of test compounds **4a-j** (2.5–80 µM) for 24 h at 37 °C in 5% CO_2. The treatment medium was then replaced with MTT in Hank's Balanced Salt Solution (HBSS) (0.5 mg/mL) for 2 h at 37 °C in 5% CO_2. After washing with HBSS, formazan crystals were dissolved in isopropanol. The amount of formazan was measured (570 nm, reference filter 690 nm) using the multilabel plate reader VICTOR™ X3 (PerkinElmer, Waltham, MA, USA). The quantity of formazan was directly proportional to the number of viable cells.

Determination of ROS Formation Induced by *t*-BuOOH

The intracellular antioxidant activity of the studied compounds induced by *t*-BuOOH was evaluated in SH-SY5Y cells as previously described [46]. The ROS formation was determined using a 2′-7′ dichlorodihydrofluorescein diacetate fluorescent probe (DCFH-DA), as previously reported by Tarozzi, 2007 [46]. Firstly, SH-SY5Y cells were seeded in a 96-well plate at 2×10^4 cells/well and incubated for 24 h at 37 °C in 5% CO_2. The treatment medium was then removed and 100 µL of DCFH-DA probe (10 µg/mL) was added to each well. After 30 min of incubation at room temperature, DCFH-DA solution was replaced with 100 µL of *t*-BuOOH (100 µM) and 100 µL of the test compounds at different concentrations (2.5–10 µM) for 30 min. In parallel, the SH-SY5Y cells were also treated with compounds for 24 h before the treatment with *t*-BuOOH. The ROS formation was measured (excitation at 485 nm and emission at 535 nm) using a multilabel plate reader (VICTOR™ X3, PerkinElmer). The antioxidant activity in terms of inhibition percentage in ROS formation induced by *t*-BuOOH, is calculated using the following formula:

$$\% \text{ of inhibition} = 100 - \left(\frac{Ptc \times 100}{100}\right)$$

where Ptc = % of increase in ROS formation induced by t-BuOOH in the presence of the studied compounds; Pt = % of increase in ROS formation induced by t-BuOOH.

Determination of Intracellular Glutathione Levels

Glutathione (GSH) levels were measured by using the fluorescent probe monochlorobimane (MCB), as previously described [47]. SH-SY5Y cells were seeded in a black 96-well plate at 2×10^4 cells/well, incubated for 24 h and subsequently treated with test compounds at different concentrations (2.5–10 µM) for 24 h at 37 °C in 5% CO_2. At the end of incubation, the treatment medium was removed and 100 µL of MCB was added to each well. After 30 min of incubation at 37 °C in 5% CO_2, GSH levels were measured

(excitation at 355 nm and emission at 460 nm) using the multilabel plate reader VICTOR™ X3 (PerkinElmer). Results are expressed as a fold increase of control cells.

Nuclear Extraction and Nrf2 Binding Activity Assay

SH-SY5Y cells were seeded in 60 mm dishes at 2×10^6 cells/dish, incubated for 24 h and subsequently treated with test compounds at 10 µM for 1, 3 and 6 h at 37 °C in 5% CO_2. At the end of incubation, cytosolic and nuclear extraction for Nrf2 nuclear translocation were performed by using Nuclear Extract Kit (Active Motif, Carlsbad, CA, USA), according to the manufacturer's guidelines. Nuclear extracts (10 µg) obtained were then used to determine the active Nrf2 protein level by using the TransAM Nrf2 Kit (Active Motif), according to the manufacturer's guidelines. The TransAM Nrf2 Kit is a DNA-binding ELISA able to determine the active Nrf2 protein level in nuclear extract. The primary antibody of the kit is able to recognize an epitope on Nrf2 protein upon ARE binding. The active Nrf2 protein levels in the treated cells are expressed as fold increase with respect to corresponding untreated cells.

$A\beta_{1-42}$ Oligomers Preparation

$A\beta_{1-42}$ peptide (AnaSpec, Fremont, CA, USA) was first dissolved in 1,1,1,3,3,3-hexafluoroisopropanol to 1 mg/mL, sonicated, incubated at room temperature for 24 h and lyophilized. The resulting unaggregated $A\beta_{1-42}$ peptide film was dissolved with DMSO and stored at −20 °C until use. The $A\beta_{1-42}$ peptide aggregation to oligomeric form ($OA\beta_{1-42}$) was prepared as previously described [48].

Neuroprotective Activity Toward $A\beta_{1-42}$ Oligomers

SH-SY5Y cells were seeded in a 96-well plate at 3×10^4 cells/well, incubated for 24 h and subsequently treated with test compounds (10 µM) and $OA\beta_{1-42}$ (10 µM) for 4 h. The neuroprotective activity, in terms of increase in intracellular MTT granules, was measured by MTT formazan exocytosis assay, as previously described [49]. Briefly, the treatment medium was replaced with MTT in HBSS (0.5 mg/mL) for 1 h at 37 °C in 5% CO_2. After the incubation, intracellular MTT granules were completely solubilized in Tween-20 (10% v/v). The absorbance of Tween-20 soluble MTT was measured at 570 nm (reference filter 690 nm) using the multilabel plate reader VICTOR™ X3 (PerkinElmer). Data are expressed as percentage of neurotoxicity versus untreated cells.

Neuroprotective Activity Toward 6-OHDA

SH-SY5Y cells were seeded in a 96-well plate at 2×10^4 cells/well, incubated for 24 h and subsequently treated with test compounds (10 µM) and 6-OHDA (100 µM) for 2 h and starved in complete medium for 22 h. The neuroprotective activity was measured by using the MTT assay as previously described [50]. Data are expressed as percentage of neurotoxicity versus untreated cells.

Neuroprotective Activity Toward 3-NP

SH-SY5Y cells were seeded in a 96-well plate at 2×10^4 cells/well, incubated for 24 h and subsequently treated with test compounds (10 µM) and 3-NP (5 mM) for 24 h. The neuroprotective activity was measured by using the MTT assay. Data are expressed as percentage of neurotoxicity versus untreated cells.

References

1. Seltzer B (2007) Donepezil: an update. Expert Opin Pharmacother 8:1011–1023. https://doi.org/10.1517/14656566.8.7.1011
2. Kumar A, Singh A (2015) A review on Alzheimer's disease pathophysiology and its management: an update. Pharmacol Rep 67:195–203. https://doi.org/10.1016/J.PHAREP.2014.09.004
3. Voon V, Napier TC, Frank MJ et al (2017) Impulse control disorders and levodopa-induced dyskinesias in Parkinson's disease: an update. Lancet Neurol 16:238–250. https://doi.org/10.1016/S1474-4422(17)30004-2
4. Knight R, Khondoker M, Magill N et al (2018) A systematic review and meta-analysis of the effectiveness of acetylcholinesterase inhibitors and memantine in treating the cognitive symptoms of dementia. Dement Geriatr Cogn Disord 45:131–151. https://doi.org/10.1159/000486546
5. Hou Y, Dan X, Babbar M et al (2019) Ageing as a risk factor for neurodegenerative disease. Nat Rev Neurol 15:565–581. https://doi.org/10.1038/s41582-019-0244-7
6. Popa-Wagner A, Dumitrascu D, Capitanescu B et al (2020) Dietary habits, lifestyle factors and neurodegenerative diseases. Neural Regen Res 15:394. https://doi.org/10.4103/1673-5374.266045
7. Lü J-M, Lin PH, Yao Q, Chen C (2010) Chemical and molecular mechanisms of antioxidants: experimental approaches and model systems. J Cell Mol Med 14:840–860. https://doi.org/10.1111/j.1582-4934.2009.00897.x
8. Dinkova-Kostova AT, Talalay P (2008) Direct and indirect antioxidant properties of inducers of cytoprotective proteins. Mol Nutr Food Res 52(1):S128–S138. https://doi.org/10.1002/mnfr.200700195
9. Ortiz CJC, de Freitas Silva M, Gontijo VS et al (2018) Design of multi-target directed ligands as a modern approach for the

development of innovative drug candidates for Alzheimer's disease. Humana Press, New York, pp 255–351
10. Benchekroun M, Romero A, Egea J et al (2016) The antioxidant additive approach for alzheimer's disease therapy: new ferulic (Lipoic) acid plus melatonin modified tacrines as cholinesterases inhibitors, direct antioxidants, and nuclear factor (erythroid-derived 2)-like 2 activators. J Med Chem 59:9967–9973. https://doi.org/10.1021/acs.jmedchem.6b01178
11. Ramsay RR, Popovic-Nikolic MR, Nikolic K et al (2018) A perspective on multi-target drug discovery and design for complex diseases. Clin Transl Med 7:3. https://doi.org/10.1186/s40169-017-0181-2
12. Dias KST, de Paula CT, dos Santos T et al (2017) Design, synthesis and evaluation of novel feruloyl-donepezil hybrids as potential multitarget drugs for the treatment of Alzheimer's disease. Eur J Med Chem 130:440–457. https://doi.org/10.1016/j.ejmech.2017.02.043
13. Fraga CAM, Barreiro EJ (2006) Medicinal chemistry of N-acylhydrazones: new lead-compounds of analgesic, antiinflammatory and antithrombotic drugs. Curr Med Chem 13:167–198. https://doi.org/10.2174/092986706775197881
14. Duarte CD, Barreiro EJ, Fraga CAM (2007) Privileged structures: a useful concept for the rational design of new lead drug candidates. Mini Rev Med Chem 7:1108–1119. https://doi.org/10.2174/138955707782331722
15. Ellman GL, Courtney KD, Andres V, Featherstone RM (1961) A new and rapid colorimetric determination of acetylcholinesterase activity. Biochem Pharmacol 7:88–95. https://doi.org/10.1016/0006-2952(61)90145-9
16. Li Q, Yang H, Chen Y, Sun H (2017) Recent progress in the identification of selective butyrylcholinesterase inhibitors for Alzheimer's disease. Eur J Med Chem 132:294–309. https://doi.org/10.1016/j.ejmech.2017.03.062
17. Kandiah N, Pai M-C, Senanarong V et al (2017) Rivastigmine: the advantages of dual inhibition of acetylcholinesterase and butyrylcholinesterase and its role in subcortical vascular dementia and Parkinson's disease dementia. Clin Interv Aging 12:697. https://doi.org/10.2147/CIA.S129145
18. Meden A, Knez D, Jukič M et al (2019) Tryptophan-derived butyrylcholinesterase inhibitors as promising leads against Alzheimer's disease. Chem Commun 55:3765–3768. https://doi.org/10.1039/c9cc01330j
19. Dighe SN, Deora GS, De la Mora E et al (2016) Discovery and structure-activity relationships of a highly selective butyrylcholinesterase inhibitor by structure-based virtual screening. J Med Chem 59:7683–7689. https://doi.org/10.1021/acs.jmedchem.6b00356
20. Košak U, Brus B, Knez D et al (2018) The magic of crystal structure-based inhibitor optimization: development of a butyrylcholinesterase inhibitor with picomolar affinity and in vivo activity. J Med Chem 61:119–139. https://doi.org/10.1021/acs.jmedchem.7b01086
21. Rosenberry T, Brazzolotto X, Macdonald I et al (2017) Comparison of the binding of reversible inhibitors to human butyrylcholinesterase and acetylcholinesterase: a crystallographic, kinetic and calorimetric study. Molecules 22:2098. https://doi.org/10.3390/molecules22122098
22. Brus B, Košak U, Turk S et al (2014) Discovery, biological evaluation, and crystal structure of a novel nanomolar selective butyrylcholinesterase inhibitor. J Med Chem 57:8167–8179. https://doi.org/10.1021/jm501195e
23. Kamat PK, Kalani A, Rai S et al (2016) Mechanism of oxidative stress and synapse dysfunction in the pathogenesis of Alzheimer's disease: understanding the therapeutics strategies. Mol Neurobiol 53:648–661. https://doi.org/10.1007/s12035-014-9053-6
24. Chen M, Du Z-Y, Zheng X et al (2018) Use of curcumin in diagnosis, prevention, and treatment of Alzheimer's disease. Neural Regen Res 13:742–752. https://doi.org/10.4103/1673-5374.230303
25. Abrahams S, Haylett WL, Johnson G et al (2019) Antioxidant effects of curcumin in models of neurodegeneration, aging, oxidative and nitrosative stress: a review. Neuroscience 406:1–21. https://doi.org/10.1016/j.neuroscience.2019.02.020
26. Cai Y-Z, Sun Mei, Xing Jie et al (2006) Structure–radical scavenging activity relationships of phenolic compounds from traditional Chinese medicinal plants. Life Sci 78:2872–2888. https://doi.org/10.1016/J.LFS.2005.11.004
27. Kim J-K, Jang H-D (2014) Nrf2-mediated HO-1 induction coupled with the erk signaling pathway contributes to indirect antioxidant capacity of caffeic acid phenethyl ester in HepG2 cells. Int J Mol Sci 15:12149–12165. https://doi.org/10.3390/ijms150712149
28. Gu F, Chauhan V, Chauhan A (2015) Glutathione redox imbalance in brain disorders. Curr Opin Clin Nutr Metab Care 18:89–95. https://doi.org/10.1097/MCO.0000000000000134
29. Dinkova-Kostova AT, Kostov RV, Kazantsev AG (2018) The role of Nrf2 signaling in counteracting neurodegenerative diseases. FEBS J 285:3576–3590. https://doi.org/10.1111/febs.14379
30. Bryan HK, Olayanju A, Goldring CE, Park BK (2013) The Nrf2 cell defence pathway: keap1-dependent and -independent mechanisms of regulation. Biochem Pharmacol 85:705–717. https://doi.org/10.1016/J.BCP.2012.11.016
31. Lalkovičová M, Danielisová V (2016) Neuroprotection and antioxidants. Neural Regen Res 11:865–874. https://doi.org/10.4103/1673-5374.184447
32. Klein W, Krafft G, Finch C (2001) Targeting small Aβ oligomers: the solution to an Alzheimer's disease conundrum? Trends Neurosci 24:219–224. https://doi.org/10.1016/S0166-2236(00)01749-5
33. Simola N, Morelli M, Carta AR (2007) The 6-hydroxydopamine model of parkinson's disease. Neurotox Res 11:151–167. https://doi.org/10.1007/BF03033565
34. Túnez I, Tasset I, La Cruz VP, De Santamaría A (2010) 3-Nitropropionic acid as a tool to study the mechanisms involved in huntington's disease: past, present and future. Molecules 15:878–916. https://doi.org/10.3390/molecules15020878
35. Lipinski CA, Lombardo F, Dominy BW, Feeney PJ (2001) Experimental and computational approaches to estimate solubility and permeability in drug discovery and development settings. Adv Drug Deliv Rev 46:3–26. https://doi.org/10.1016/S0169-409X(00)00129-0
36. Cheung J, Rudolph MJ, Burshteyn F et al (2012) Structures of human acetylcholinesterase in complex with pharmacologically important ligands. J Med Chem 55:10282–10286. https://doi.org/10.1021/jm300871x
37. Lopes JPB, Silva L, Ceschi MA et al (2019) Synthesis of new lophine–carbohydrate hybrids as cholinesterase inhibitors: cytotoxicity evaluation and molecular modeling. Medchemcomm 10:2089–2101. https://doi.org/10.1039/C9MD00358D
38. Chalupova K, Korabecny J, Bartolini M et al (2019) Novel tacrine-tryptophan hybrids: multi-target directed ligands as potential treatment for Alzheimer's disease. Eur J Med Chem 168:491–514. https://doi.org/10.1016/j.ejmech.2019.02.021
39. Madhavi Sastry G, Adzhigirey M, Day T et al (2013) Protein and ligand preparation: parameters, protocols, and influence on virtual screening enrichments. J Comput Aided Mol Des 27:221–234. https://doi.org/10.1007/s10822-013-9644-8
40. Greenwood JR, Calkins D, Sullivan AP, Shelley JC (2010) Towards the comprehensive, rapid, and accurate prediction of the favorable tautomeric states of drug-like molecules in aqueous solution. J Comput Aided Mol Des 24:591–604. https://doi.org/10.1007/s10822-010-9349-1

41. Friesner RA, Banks JL, Murphy RB et al (2004) Glide: a new approach for rapid, accurate docking and scoring. 1. method and assessment of docking accuracy. J Med Chem 47:1739–1749. https://doi.org/10.1021/jm0306430
42. Santos SN, Alves de Souza G, Pereira TM et al (2019) Regioselective microwave synthesis and derivatization of 1,5-diaryl-3-amino-1,2,4-triazoles and a study of their cholinesterase inhibition properties. RSC Adv 9:20356–20369. https://doi.org/10.1039/C9RA04105B
43. de Souza GA, da Silva SJ, de Cistia CN et al (2019) Discovery of novel dual-active 3-(4-(dimethylamino)phenyl)-7-aminoalcoxy-coumarin as potent and selective acetylcholinesterase inhibitor and antioxidant. J Enzyme Inhib Med Chem 34:631–637. https://doi.org/10.1080/14756366.2019.1571270
44. Gontijo VS, De Souza TC, Rosa IA et al (2012) Isolation and evaluation of the antioxidant activity of phenolic constituents of the Garcinia brasiliensis epicarp. Food Chem 132:1230–1235. https://doi.org/10.1016/j.foodchem.2011.10.110
45. Rampa A, Bartolini M, Pruccoli L et al (2018) Exploiting the chalcone scaffold to develop multifunctional agents for Alzheimer's disease. Molecules 23:1902. https://doi.org/10.3390/molecules23081902
46. Tarozzi A, Morroni F, Hrelia S et al (2007) Neuroprotective effects of anthocyanins and their in vivo metabolites in SH-SY5Y cells. Neurosci Lett 424:36–40. https://doi.org/10.1016/j.neulet.2007.07.017
47. Sebastià J, Cristòfol R, Martín M et al (2003) Evaluation of fluorescent dyes for measuring intracellular glutathione content in primary cultures of human neurons and neuroblastoma SH-SY5Y. Cytom Part A 51A:16–25. https://doi.org/10.1002/cyto.a.10003
48. Tarozzi A, Bartolini M, Piazzi L et al (2014) From the dual function lead AP2238 to AP2469, a multi-target-directed ligand for the treatment of Alzheimer's disease. Pharmacol Res Perspect 2:e00023. https://doi.org/10.1002/prp2.2349
49. Dias Viegas FP, de Freitas Silva M, Divino da Rocha M et al (2018) Design, synthesis and pharmacological evaluation of N-benzyl-piperidinyl-aryl-acylhydrazone derivatives as donepezil hybrids: discovery of novel multi-target anti-alzheimer prototype drug candidates. Eur J Med Chem 147:48–65. https://doi.org/10.1016/J.EJMECH.2018.01.066
50. Morroni F, Sita G, Djemil A et al (2018) Comparison of Adaptive Neuroprotective Mechanisms of Sulforaphane and its Interconversion Product Erucin in *in Vitro* and *in Vivo* Models of Parkinson's Disease. J Agric Food Chem 66:856–865. https://doi.org/10.1021/acs.jafc.7b04641

Affiliations

Cindy Juliet Cristancho Ortiz[1] · Caio Miranda Damasio[1] · Letizia Pruccoli[2] · Nathália Fonseca Nadur[3] · Luciana Luiza de Azevedo[3] · Isabella Alvim Guedes[4] · Laurent Emmanuel Dardenne[4] · Arthur Eugen Kümmerle[3] · Andrea Tarozzi[2] · Claudio Viegas Jr.[1]

✉ Andrea Tarozzi
andrea.tarozzi@unibo.it

✉ Claudio Viegas Jr.
cvjviegas@gmail.com

[1] PeQuiM-Laboratory of Research in Medicinal Chemistry, Federal University of Alfenas, Jovino Fernandes Sales Avenue 2600, Alfenas, MG 37130-840, Brazil

[2] Department for Life Quality Studies, Alma Mater Studiorum-University of Bologna, Corso d'Augusto 237, 47921 Rimini, Italy

[3] Laboratory of Molecular Pharmacology, Institute of Biomedical Sciences, Federal University of Rio de Janeiro, Rio De Janeiro, RJ 21941-902, Brazil

[4] National Laboratory of Scientific Computation, Petrópolis, RJ 25651-075, Brazil